Sulfidation State of Fluids in Active and Extinct Hydrothermal Systems: Transitions from Porphyry to Epithermal Environments

Marco T. Einaudi[1]
Department of Geological and Environmental Sciences
Stanford University
Stanford, California 94305-2115

Jeffrey W. Hedenquist
Department of Geology and Geological Engineering
Colorado School of Mines
Golden, Colorado 80401-1887

E. Esra Inan
Department of Geological and Environmental Sciences
Stanford University
Stanford, California 94305-2115

Running title: Sulfidation state of hydrothermal fluids

In Press: Giggenbach Volume, Society of Economic Geologists and Geochemical Society,

Special Publication 10 (S.F. Simmons, ed.)

[1] corresponding author, e-mail: marco@pangea.stanford.edu

Abstract

Use of the concept of "sulfidation state", in parallel with oxidation state, in the study of ore deposits finds its beginnings with the studies of Reno Sales and Charles Meyer at Butte, Montana. Experimental determination of the stability of sulfide minerals in terms of fS_2 and temperature followed, leading to definition of contrasts in ore-forming environments. More recent studies of vapor compositions in active volcanic and geothermal systems allow direct comparisons with geochemical environments deduced from petrologic study. In this paper, we present a compilation of oxidation and sulfidation states of fresh igneous rocks from arc environments and on sulfidation states of sulfide assemblages in calc-alkalic porphyry copper, porphyry-related base-metal veins, and epithermal gold-silver deposits. These data are contrasted with compositions of fluids from active systems by plotting vapor compositions on $\log fS_2$ – $1000/T$, R_H – $1000/T$, R_S – $1000/T$ diagrams, where $R_H \approx \log (X_{H_2} / X_{H_2O})$, $R_S \approx \log (X_{H_2} / X_{H_2S})$ and X = mole fraction of the gas.

Oxidation states of andesitic arc magmas plot in a tight cluster between fayalite + magnetite + quartz and pyrrhotite + pyrite + magnetite. On equilibrating below the solidus, arc plutons deviate toward higher oxidation states. Sulfidation states of arc magmas are very low to

low, lying between fayalite + magnetite + quartz + pyrrhotite and pyrrhotite + pyrite. A plot of R_H values versus measured temperatures for volcanic fumaroles reveals close agreement with the isomolar $SO_2 = H_2S$ curve (sulfur-gas buffer) to temperatures below 500 °C. Giggenbach concluded from this observation that the oxidation state of the vapors is controlled by their magmatic sulfur-gas composition, a conclusion consistent with oxidation state trajectories for cooling plutons.

Reactive magmatic-hydrothermal fluids from active systems trend toward lower R_H and R_S (higher oxidation and sulfidation states) with declining temperature, achieving minima at 200 to 100°C (R_S = -1.5 to –3.0). Below 200 °C, R_H and R_S both increase abruptly (R_S =0) through interaction with wall rock. In contrast, geothermal liquids are relatively reduced, near neutral pH, and their sulfidation state remains low to intermediate (R_S =0) throughout the range 320-100°C. This may be caused by a greater degree of fluid-rock interaction at depth, a smaller magmatic component, or a distinct magmatic component. The reduced limit of geothermal compositions has an R_H value of about –3, equivalent to Giggenbach's rock buffer, where iron-bearing minerals in fresh rock establish a "floor" to the oxidation state, just as the sulfur-gas buffer acts as a "ceiling".

The majority of porphyry copper deposits contain magnetite, either without sulfides or as part of ore-grade assemblages containing bornite and/or chalcopyrite without pyrite. In some deposits, pyrite + chalcopyrite dominates the ore zone. All of these assemblages are of intermediate sulfidation state. High-temperature volcanic fumaroles plot largely in the bornite + magnetite field, consistent with the view that porphyry copper assemblages precipitate from magmatic volatiles that cooled along the sulfur-gas buffer. Base-metal veins associated with porphyry copper deposits extend this cooling trend and display a range of sulfidation states from very high in central zones (pyrite + digenite + covellite + enargite) to intermediate and low in peripheral zones or latest stages (pyrite + tennantite + chalcopyrite).

In high-sulfidation (HS) epithermal deposits the sulfidation state ranges from high for copper-rich enargite-bearing assemblages to intermediate for the later gold-rich tennantite-tetrahedrite + pyrite assemblages, with similarities to and overlap with the base-metal veins. In intermediate sulfidation (IS) epithermal deposits the full range of intermediate sulfidation states is represented by the assemblage pyrite + chalcopyrite + tetrahedrite. The general similarity of assemblages associated with gold in HS and IS deposits suggests a closer affiliation between these two types than commonly thought. Low sulfidation (LS) epithermal deposits appear to be distinct and show little variation from low and intermediate sulfidation states. Evidence for transients in sulfidation state, due to boiling, local wall rock influence, or other factors, exists in all three types of epithermal deposits.

Sulfide mineral assemblages in porphyry copper deposits, porphyry-related base-metal veins, and HS-IS epithermal deposits, when taken together, describe a cooling path toward increasing sulfidation states from R_S = -1 at 600ºC to R_S = -3 at 300ºC, followed by an abrupt increase to R_S = 0 as equilibrium with the rock buffer is achieved. This pattern, also evident in fluid compositions from active magmatic-hydrothermal systems, suggests a continuum between these deposit types. Fluid compositions in active hydrothermal systems span the complete range of chemical and physical states that are commonly relegated to changing time in intrusion-centered ore deposits.

Introduction

Analogies have long been made between active and extinct hydrothermal systems in the study of ore deposits, first in the early part of the 20th C in the context of epithermal deposits (Ransome, 1907; Lindgren, 1933). In porphyry-type deposits, analogies evolved from dominantly geological (e.g., Sillitoe, 1973), through dominantly physical (e.g., Henley and McNabb, 1978), to integrative (White, 1981; Hedenquist and Lowenstern, 1994) as the data base on geology and fluid composition in active systems expanded (e.g., Henley and Ellis, 1983; Giggenbach, 1997).

The geochemical pathways taken by hydrothermal fluids can be described in terms of many variables. One that has long spanned the disciplines of economic geology, petrology and geochemistry is oxidation state (fO_2 compared to a standard), a variable of particular importance because of its effect on the speciation of sulfur in magmas and in aqueous fluids and its role in metal transport (Barnes and Czamanske, 1967; Burnham, 1979; Burnham and Ohmoto, 1980; Candela, 1992). Oxidation state can be estimated from mineral assemblages in igneous rocks (e.g., Wones, 1981; Whitney, 1984) and ore deposits (Holland, 1959; Barnes and Kullerud, 1961; Meyer and Hemley, 1967), and calculated from direct sampling in active systems (Giggenbach, 1987). The application of sulfur fugacity (or less precisely, partial pressure) migrated into the geologic realm from metallurgy about the middle of the last century and its application to ores (e.g., Merwin and Lombard, 1937; Sales and Meyer, 1949; McKinstry, 1959) closely paralleled the use of oxygen fugacity in petrology. Sulfidation state, a function of both fS_2 and temperature (Barton and Skinner, 1967; Barton, 1970) has had limited application to the classification of ore deposits (e.g., Heald et al., 1987) and the study of continua within classes (e.g., Barton et al., 1995) despite the consistent framework it provides for systematizing sulfide mineral assemblages and studying evolution of hydrothermal systems.

In this paper, our focus is on ores related to medium-K and high-K calc-alkaline magmatic suites of both continental and oceanic arc environments. We consider deep porphyry-copper environments as transitional into shallower porphyry-related base-metal vein and replacement deposits (Meyer and Hemley, 1967; Einaudi, 1982; Hemley and Hunt, 1992) and ultimately near the surface into epithermal gold-silver deposits (Sillitoe, 1973; Sillitoe, 1983; Hedenquist et al., 1998; Muntean and Einaudi, 2001). If taken as a whole, sulfide mineral assemblages in these deposits describe a "Lazy-L" shaped field on a $\log fS_2$ – 1000/T diagram (Fig. 1). In a given district, such a field would represent the integrated evolutionary paths of multiple batches of hydrothermal fluids, likely from different sources, as they undergo cooling, depressurization, and variable degrees of interaction with their wall rocks. The environment described is one of increasing sulfidation state on cooling from near magmatic temperatures down to 300°C, at which point an abrupt decline in sulfidation state occurs. This same Lazy-L pattern was deduced 35 years ago by Meyer and Hemley (1967), yet the analogy with fluid pathways in active volcanic and geothermal systems was not appreciated at that time due to a paucity of reliable analytical data on fluids. As discussed in this paper, fluids from active systems (e.g., compilations by Giggenbach et al., 1986, Giggenbach, 1996, and references therein) mimic this L-shaped trend in both sulfidation and redox states.

We first summarize aspects of terminology and the oxidation and sulfidation state of magmas and wall rocks, then present an overview of the fluid chemistry of active hydrothermal systems and compare this to the evidence from mineral assemblages in ore deposits. We touch on processes that control the pathways of fluid evolution based on our integration of information from these active and extinct systems.

Terminology and Conventions

Mineral assemblages, associations, and zoning

Mineral assemblages commonly are defined as groupings of minerals that occur in direct contact and that do not display evidence of reaction with one another (Barton et al., 1963). The term mineral association is applied to groups of minerals that are characteristic of a given zone of alteration or portion of a vein system, but which are not all in contact and were not necessarily all deposited at the same time. Thus, pyrite, chalcopyrite, bornite, and magnetite is a common association in potassic alteration zones in porphyry copper deposits, but the assemblages are magnetite + bornite, bornite + chalcopyrite, or chalcopyrite + pyrite, but not bornite + pyrite in this environment. In the text below minerals that are part of an assemblage are joined with plus signs, and minerals that are part of an association are separated by commas.

Although mineral associations commonly are summarized in maps showing mineral zoning, such maps are ambiguous because they represent patterns resulting from superposition of multiple packets of fluids and migrating flow paths through time. To serve as a basis for assessment of processes (and for ore finding), such maps need to be redrawn as a series of time frames representing the zoning of mineral assemblages at given points in time. In order to draw time frames, it is necessary to map time lines through the deposit. In porphyry deposits, successive intrusions can serve as time lines to draw successive time-frames (e.g., Gustafson and Hunt, 1975; Carten, 1986; Dilles and Einaudi, 1992) or space-time diagrams (Dilles et al., 2000; Muntean and Einaudi, 2001). In vein deposits, time lines are more difficult to establish, but in some cases these can be based on the presence of unique features such as sphalerite stratigraphy (Barton et al., 1977; Hayba, 1997).

In spite of these ambiguities in the link between space and time, some common themes are evident within the deposit types considered here. For example, in the early stages of zoned base-metal veins found in some porphyry copper districts, minerals occurring in innermost zones appear to have encroached outward onto minerals that comprised the next outer zones. In some deposits (e.g., Main Stage veins at Butte, Montana: Sales and Meyer, 1949) this contemporaneous zonal growth pattern was largely frozen in (prograde pattern). In other deposits, minerals of the outer zones encroached onto the center of the deposit as isotherms collapsed, and it is this late stage that is most prominently recorded by the temporal sequence of minerals, especially sulfides (retrograde pattern). This time sequence may be seen in outcrop as late pyrite veins cutting early quartz + chalcopyrite + bornite veins in many porphyry copper deposits (e.g., El Salvador, Chile; Gustafson and Hunt, 1975) or recognized under the microscope as late tennantite replacing enargite in many base-metal veins (e.g., McKinstry, 1963) and in some high-sulfidation epithermal gold deposits (e.g., Jannas et al., 1999; Claveria, 2001). These and other issues related to zoning and paragenesis and the use of paragenetic diagrams have been reviewed by Hemley and Hunt (1992, p. 36-40). In the present paper, we summarize these spatial and temporal patterns in tables and plot trends on phase diagrams. The plotted trends are representative of the geochemical environments within cooling hydrothermal systems and do not in general represent the trajectory of a single episode of hydrothermal fluid flow. In some districts these changing environments are spatially separated (e.g., an outward zonal pattern such as A-B-C, Fig. 1), in others they are superimposed (e.g., B superimposed on A, followed by C superimposed on B, Fig. 1), but we have not attempted to make this distinction on phase diagrams.

Sulfidation state terminology

The terms "sulfidation" and "sulfidation state", and the concepts that surround them, have a long history of development in the study of ore deposits. Table 1 serves to record part of that history and to define and clarify the terminology. The references cited are among the highlights, but are not intended as a comprehensive review. The large number of terms involved, including "high-sulfur sulfides", "sulfidation", "sulfidation reactions", "sulfur fugacity", and "sulfidation state", often are used as synonyms, whereas they have different meanings (Table 1).

We use the term sulfidation state as defined by Barton (1970) and in a manner analogous to oxidation state (e.g., Wones, 1981), where the frame of reference is temperature and the fugacity of S_2 and O_2 gas, respectively. The sulfur or oxygen fugacity of a system at any temperature can be compared to standard mineral reactions (buffers), such as

$$4 Fe_3O_4 + O_2 = 6 Fe_2O_3 \qquad (1)$$

magnetite　　　hematite

for oxygen, or

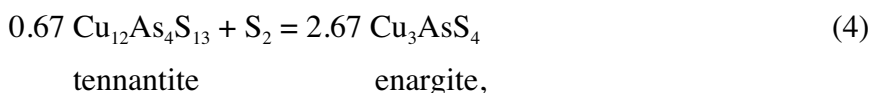$$2 FeS + S_2 = 2 FeS_2 \qquad (2)$$

pyrrhotite　　pyrite

for sulfur. The difference between the oxygen or sulfur fugacity implied by a natural mineral assemblage compared with that of a buffer reaction forms the basis for assigning relative oxidation or sulfidation states.
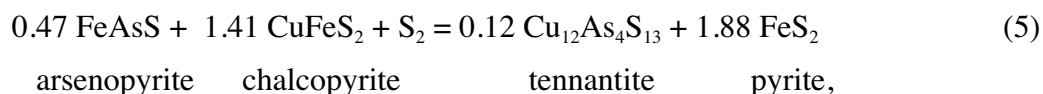
For ease of comparing the sulfidation state between different fluids and between fluids and mineral assemblages, we introduce here an informal terminology based on sulfidation reactions among minerals in the system Cu-Fe-As-S (reactions identified in Fig. 1) common to porphyry copper deposits, porphyry-related veins, and epithermal precious-metal deposits. From low to high, these are: "very low", "low", "intermediate", "high", and "very high" sulfidation states. The boundary between intermediate and high sulfidation states is defined by the sulfidation reaction

$$5 CuFeS_2 + S_2 = Cu_5FeS_4 + 4 FeS_2 \qquad (3)$$

chalcopyrite　　　bornite　　　pyrite,
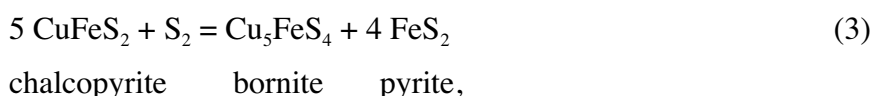
(Fig. 1) which approximately coincides with the sulfidation reaction

$$0.67 Cu_{12}As_4S_{13} + S_2 = 2.67 Cu_3AsS_4 \qquad (4)$$

tennantite　　　　　　　enargite,

and represents the transition between porphyry copper deposits (*sensu stricto*) and porphyry-related base-metal veins (see below). Further, the sulfidation reaction

$$0.47 FeAsS + 1.41 CuFeS_2 + S_2 = 0.12 Cu_{12}As_4S_{13} + 1.88 FeS_2 \qquad (5)$$

arsenopyrite　　chalcopyrite　　　　tennantite　　　pyrite,

representing a lower limit to sulfidation state in IS epithermal deposits, effectively coincides with the lower limit of intermediate sulfidation states as defined by the reaction (2).

Sulfidation state is neither a function of the sulfur content of a sulfide mineral or mineral assemblage, nor a function of proximity of a given assemblage or fluid to the sulfur condensation

curve. Regarding the first point, pyrite contains more sulfur than covellite, but its stability field extends to lower sulfidation states than that of covellite (Fig. 1). Regarding the second point, the sulfur condensation curve, which acts as a ceiling to fS_2 at any given temperature, has a flatter slope on a log fS_2 - (1000/T) diagram than the sulfidation reactions used here to index sulfidation state (Fig. 1). Because of this relation, each sulfidation state has an upper thermal limit.

We caution that the term sulfidation state is not strictly parallel to the terms "high sulfidation" (HS) and "low sulfidation" (LS) used in the classification of epithermal deposits (White and Hedenquist, 1990; Hedenquist et al., 1994a; Table 1), although sulfide assemblages that characterize the major portion of many epithermal deposits (e.g., enargite in HS deposits) are mostly consistent with the classification terms. Sulfidation state, as used here in the sense of a mineral facies or in the context of mineral assemblages and fluids, can vary widely within deposits, and, as pointed out by Barton (1970), can vary within a hand sample or crystal.

Different, hypothetical cooling paths can be drawn on a log fS_2 – 1000/T petrogenetic grid: gas-buffered, rock-buffered, and mineral-buffered paths. The latter two types of cooling paths are treated at length below. A mineral-buffered path is one that is parallel to mineral reaction lines – cooling takes place at constant sulfidation state, although the absolute value of fS_2 declines along such a path. As stressed by Barton (1970), hydrothermal fluids rarely follow mineral-buffered paths, the mineral buffers being more correctly regarded as indicators of the state of the system at a given point in space and time. Barton's (1970) Main Line environment (Fig. 1), representing the common range of sulfidation states in ore-forming hydrothermal systems and containing an infinite number of possible fluid trajectories, has a lower positive slope than mineral buffers on a log fS_2 – 1000/T diagram. Thus, this environment is one of gradually increasing sulfidation state (although the value of fS_2 decreases) with decreasing temperature. One of the key themes of the present paper is to investigate such trajectories in natural ores and active hydrothermal systems.

Relationship between sulfidation state, oxidation state, and pH

The valence state of sulfur was the basis used by Hedenquist (1987) in the original definition of two end member "high sulfidation" and "low sulfidation" epithermal deposits (Table 1). Aqueous and gas species in ore-forming fluids contain sulfur in valence, or oxidation, states (n) that are either greater (e.g., in $SO_4^=$, n = +2) or less (in H_2S, n = -2) than S_2 (n = 0). With this measure of oxidation state, two oxidation states can apply to a single sulfidation state depending on whether the predominant aqueous species is sulfate or sulfide. However, if fO_2 is used as a measure of oxidation state, as in this paper, then in H_2S-dominant fluids fS_2 covaries with fO_2:

$$2 H_2S + O_2 = S_2 + 2 H_2O, \tag{6}$$

and in $SO_4^=$-dominant fluids fS_2 is inversely proportional to the cube root of fO_2 at constant pH:

$$2 SO_4^= + 4 H^+ = S_2 + 3 O_2 + 2 H_2O. \tag{7}$$
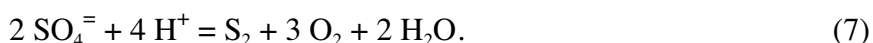
In the commonly recognized isothermal log fS_2 -log fO_2 and log fO_2 – pH plots, the above relations are expressed by a maximum in fS_2 that lies along the aqueous sulfate-sulfide predominance boundaries, where fS_2 increases with increasing fO_2 and decreasing pH (see figures and discussion in Barnes and Kullerud, 1961; Barnes and Czamanske, 1967). Meyer and Hemley (1967, p. 222) use equations such as (6) and (7) above to stress the "delicate relationships" between fS_2 and fO_2 and pH, in which relatively low pH correlates with relatively

high fugacities of both sulfur and oxygen (e.g., reaction 7) at high ratios of $f\mathrm{S}_2/f\mathrm{O}_2$, a correlation amply supported by sulfide-silicate assemblages in ore deposits.

R_S and R_H as alternative expressions of sulfidation and oxidation state

Given the complex relationships just described between $f\mathrm{S}_2$, $f\mathrm{O}_2$, pH, and aqueous sulfur species, and given the low concentrations of S_2 gas below 600ºC, it can be argued that analysis of geochemical systems is better conducted on the basis of actual reaction participants. Thus, Giggenbach (1987) adopted the redox parameter $R_H = \log(f\mathrm{H}_2 / f\mathrm{H}_2\mathrm{O})$, and the sulfidation state parameter $R_S = \log(f\mathrm{H}_2 / f\mathrm{H}_2\mathrm{S})$. The variables R_S and $\log f\mathrm{S}_2$ (and R_H and $\log f\mathrm{O}_2$) are equally valid representations of phase equilibria. We use both representations and retain $f\mathrm{S}_2$ because of its historical use in the study of ore deposits and its thermodynamic importance in the definition of sulfide phase equilibria. The final story is best told with a combination of both sets of variables.

Vapor compositions from active hydrothermal systems can be plotted directly on R_H – 1000/T, R_S – 1000/T, and $\log f\mathrm{S}_2$ – 1000/T diagrams where $R_H \approx \log(X\mathrm{H}_2 / X\mathrm{H}_2\mathrm{O})$, $R_S \approx \log(X\mathrm{H}_2 / X\mathrm{H}_2\mathrm{S})$, and X = analytical mole fraction (Appendix). We have vertically flipped the R_H – 1000/T and R_S – 1000/T diagrams from Giggenbach's original orientation so that the values of R_H and R_S increase downward on the y-axis. In this view, the topology is similar to the $\log f\mathrm{O}_2$ - 1000/T and $\log f\mathrm{S}_2$ - 1000/T diagrams, respectively, typically used in petrology and ore deposit studies (Fig. 2). As discussed below, vapors from active systems define a pattern similar to the Lazy-L defined by sulfide assemblages of porphyry and epithermal affiliation (compare Figs. 1 and 2).

Magmas, Rock Buffers, and Gas Buffers

Oxidation and sulfidation states of magmas

Here we briefly summarize data on oxidation and sulfidation state of magmas because these are the starting points for consideration of magmatic volatiles. The correlation between oxidation state of magmas and the types of associated mineral deposits has been addressed in the context of porphyry- and granitoid-related deposits (Burnham and Ohmoto, 1980; Einaudi et al., 1981; Thompson and Newberry, 2000), and in the broader perspective of igneous controls on metallogenesis (Ishihara, 1981; Barton et al., 1995; Barton, 1996; Jensen and Barton, 2000; John, 2001).

The oxidation state of magmas can be estimated on the basis of mineral associations and contrasts in ferric/ferrous ratios or magnetic susceptibility. These qualitative approaches to oxidation state, useful in metallogenetic analysis (e.g., Ishihara, 1981; Thompson and Newberry, 2000), are insufficient for our purpose, which is to compare quantitative estimates with analytical data from active hydrothermal systems. For quantitative estimates of oxidation states the compositions of coexisting ilmenite and titano-magnetite are particularly useful (Buddington and Lindsley, 1964; Haggerty, 1976; Spencer and Lindsley, 1981; Hildreth, 1981), but also important are assemblages containing iron-magnesium silicates and titanite (Wones, 1981; Dilles, 1987; Andersen et al., 1991). The continuing refinement of solution models for Fe-Ti-oxides, pyroxene and olivine (Andersen et al., 1993) means that past compilations of the oxidation state of volcanic rocks (e.g., Haggerty, 1976) must be recalculated for internal consistency. Table 2 summarizes the sources of data used here to calculate the oxidation state of magmas and plutonic

rocks from arc and rift environments plotted on Figure 3. The result is not fundamentally different from the well-known tendency for arc magmas to lie at higher oxidation states than rift magmas (Hildreth, 1981; John, 2001). The former include the arc-related calc-alkaline magmas associated with copper-rich porphyry and base- and precious metal vein deposits worldwide and which are the focus of this paper. These arc magmas lie 2 R_H units above the hematite + magnetite buffer where the SO_2/H_2S fugacity ratio of magmatic-hydrothermal fluids ranges from 0.1 to 10 (Burnham and Ohmoto, 1980). Rift magmas include basalt and rhyolite of the Snake River and Yellowstone hotspots (Hildreth, 1981) and the Northern Nevada Rift (John, 2001) that straddle the quartz + magmatite + fayalite buffer (Fig. 3).

The sulfidation state of magmas is more difficult to estimate and has received less attention than oxidation state because sulfides rarely preserve their magmatic identities on cooling below solidus temperatures. Sulfidation states, mostly from andesitic arc environments, and approximated by the composition of pyrrhotite in magmatic sulfide combined with temperature estimates from Fe-Ti-oxides (Whitney and Stormer, 1983; Whitney, 1984; Drexler and Munoz, 1988), are plotted on Figures 4 and 5 (Table 2). Arc magmas lie between the fayalite + magnetite + quartz + pyrrhotite buffer and the pyrrhotite + pyrite + $s_{(liq)}$ invariant point, at very low to low sulfidation states (Fig. 4). Recent study of magmatic Cu-Fe-sulfide blebs in intermediate to felsic plutonic and volcanic rocks of the Great Basin, western USA (Keith et al., 1995; Keith et al., 1997; Borrock et al., 1999) are consistent with these relatively low sulfidation states, appropriate for pyrrhotite + intermediate solid solution (which incorporates the chalcopyrite composition at high temperatures), and bornite solid solution + magnetite.

"Rock buffer"

The "rock buffer" can be described as the sum of rock-forming minerals that interact with a hydrothermal fluid at sub-magmatic temperatures and mediate its sulfidation-oxidation state and total acidity (Barton, 1970; Hemley and Hunt, 1992). Minerals that are likely to be involved as buffers are the ferromagnesian minerals with iron in different valence states: Fe^{+2} in pyroxene, olivine, biotite, and magnetite; Fe^{+3} in biotite and magnetite. Giggenbach (1987) commented on the problem of defining a rock buffer in volcanic-hosted hydrothermal systems: "In the absence of detailed information on the buffer mineralogy…, it appears unjustified to presuppose the presence of any of these minerals" (p. 148). He concluded that the method used by Fudali (1965) and Carmichael and Ghiorso (1986) for estimating oxidation state of andesitic magmas can be extended to rocks, and he used fayalite and hematite as thermodynamic proxies for the rock buffer (Appendix), labeled the "Giggenbach rock buffer" on Figure 3.

Where does the Giggenbach rock buffer lie relative to mineral buffers? At 350°C, the rock buffer lies close to magnetite + pyrrhotite + pyrite; at 500°C it coincides with both Ni + NiO and K feldspar + quartz + magnetite + phlogopite ($X_{Fe}^{bio} = 0.2$), and at 800 to 1000°C it intersects the center of the field of oxidation states of subduction-related arc magmas (Figs. 2 and 3). R_H values of neutral-pH geothermal fluids lie on or slightly below this rock buffer, as discussed below. Using the above relations, we show the approximate location of the rock buffer on the $\log f S_2 - 1000/T$ and $R_S - 1000/T$ diagrams (Figs. 2, 4 and 5), where it lies in the lowermost part of Barton's (1970) Main Line sulfidation environment.

Just as magmas ranging from MOR basalt to continental arc dacite display oxidation states that vary over 3 units R_H (Fig. 3) and 2.5 units R_S (Fig. 5), the rock buffer in any given mineral deposit can deviate from the Giggenbach rock buffer. For example, the reaction of

peridotite to serpentinite could act to buffer hydrothermal fluids to low oxidation states, resulting in low sulfidation state assemblages in the initial stages of ore deposition, as at the Mamut porphyry copper deposit, Malaysia, where chalcopyrite ore contains pyrrhotite and magnetite (Kosaka and Wakita, 1978). Alternatively, quartzite lacks buffering capacity in terms of both fO$_2$ and fS$_2$; a magmatic-hydrothermal fluid traveling through quartzite could evolve along the sulfur-gas buffer (see below) toward high-sulfidation states at relatively high temperatures, as at the Bingham porphyry copper deposit, Utah (Inan and Einaudi, 2002).

Magmatic sulfur-gas buffer

The SO$_2$/H$_2$S gas ratio of volatiles exsolved from relatively oxidized, I-type magmas ranges from 0.1 to 10 (Ohmoto and Rye, 1979; Burnham and Ohmoto, 1980; Whitney and Stormer, 1983; Whitney, 1984; Giggenbach, 1987). These gases may control the oxidation/sulfidation state of hydrothermal fluids to temperatures as low as 350ºC if the sulfur gases dominate over H$_2$ and if the fluid does not react with its wall rocks due to high flow-velocities and restriction to major fissures. On the other hand, the ratio may increase on phase separation due to loss of H$_2$S and H$_2$ to the vapor or due to sulfide deposition, or may decrease as a result of chemical exchange with wall rocks containing ferrous iron or carbonaceous matter (Ohmoto and Rye, 1979). As discussed below, R$_H$ values of volcanic fumaroles above 500ºC lie close to the isomolar sulfur-gas buffer where SO$_2$/H$_2$S = 1.0. Below 500-400ºC the compositions of volcanic fumaroles and modern magmatic hydrothermal fluids are modified by partial reaction with ferrous iron in wall rocks (Giggenbach, 1987). At 250ºC in neutral pH epithermal environments the SO$_2$/H$_2$S gas ratios are in the range 10^{-6} to 10^{-4} (Barton et al., 1977) and the sulfur-gas buffer no longer applies.

Oxidation and sulfidation states of fluids in cooling plutons

Volatiles that exsolve from and are in equilibrium with andesitic magmas at 800°C are at a low sulfidation state, although mostly within four log units fS$_2$ of sulfur saturation (Figs. 2A and 4), are relatively oxidized and straddle the sulfur-gas buffer (Fig. 3). If such fluids cool in equilibrium with their host rock (roughly the R$_H$ = -3 and R$_S$ = 0 isopleths, Figs. 3, 4, and 5; see below), their sulfidation state increases only gradually, crossing into intermediate sulfidation states as pyrrhotite is succeeded by pyrite at around 300°C. Such a path approximates the "geothermal" path shown in these figures. In contrast, if magmatic volatiles cool along the sulfur-gas buffer they pass into intermediate sulfidation states at much higher temperatures, around 500°C, where magmatic sulfide blebs of pyrrhotite + intermediate solid solution are converted to pyrite + chalcopyrite. At lower temperatures, near 350°C, magnetite is oxidized and sulfidized to hematite + pyrite (Figs. 4 and 5). The few published data on oxidation states of plutonic rocks that have equilibrated to temperatures as low as 400°C (Dilles, 1987; Cornejo and Mahood, 1997; Core et al., 2001) suggest that sub-solidus cooling occurred along the sulfur-gas buffer (Fig. 3), but there is an uncertainty of unknown magnitude in extrapolating the Fe-Ti-oxide geobarometer to such oxidized conditions at these low temperatures.

Active Hydrothermal Systems

The petrologic studies discussed above used thermodynamic calculations to determine variables such as fO$_2$, fS$_2$, and pH from observed mineral assemblages. In contrast, fluids collected from active hydrothermal systems allow the reactants to be measured directly, thereby eliminating the need for detailed thermodynamic calculation. For example, the ratio XH$_2$/XH$_2$O of

a fumarole sample reflects the oxidation state of the fluid, as these components are the principal redox reactants. Furthermore, the ratio X_{H_2}/X_{H_2S} reflects the sulfidation state and can be directly related to sulfide and oxide mineral assemblages through reactions incorporating these species rather than O_2 and S_2.

Volcanic fumaroles – magmatic discharges and the S-gas buffer

On exsolution from a magma, an aqueous fluid may consist of a single phase of intermediate salinity fluid, or, if the fluid has intersected its solvus, it will comprise a low-salinity vapor and a dense, hypersaline liquid (Henley and McNabb, 1978; Shinohara, 1994). The vapor, being more buoyant, separates and rises to the surface from its high-pressure source, eventually discharging as a fumarole if it is not condensed by absorption into ground water or by cooling at low water:rock ratios. Such expansion from high to low pressure results in adiabatic cooling, typically of the order of 100°C (Giggenbach, 1987). A plot of log (X_{H_2}/X_{H_2O}), or R_H, values (Table 3) versus measured temperatures (Fig. 3, black stars) reveals that volcanic fumaroles plot close to the sulfur-gas buffer, approximately one unit R_H above arc magmas and plutons at ~500 to >1000°C. The volcanic fumarole data, plotted at measured surface temperatures, could be corrected to their original higher temperatures, where they would lie on sulfur-gas buffer curves at higher pressures and overlap more closely the field of arc magmas.

The close relationship between X_{H_2}/X_{H_2O} ratios in volcanic fumaroles and the sulfur-gas buffer (Fig. 3) extends to temperatures below 500 °C, an observation indicating that the SO_2 and H_2S concentrations control the oxidation state of the vapors as they cool (Ohmoto and Rye, 1979; Burnham and Ohmoto, 1980; Giggenbach, 1987). Magmatic vapors do not plot at more oxidized values than the sulfur-gas buffer, suggesting that this is a significant limiting condition, at least at high temperatures. The resulting R_S values decline from 1.0 to –1.5 over the sampled temperature range of 1000 to 400°C, consistent with very low to low sulfidation states within the pyrrhotite stability field, as defined in the previous section.

Magmatic-hydrothermal and geothermal systems - departure from S-gas buffer

We consider two end-member environments of intrusion-driven, active hydrothermal systems below 500°C: magmatic hydrothermal and geothermal (Table 3). Surficial vapors discharged from boiling magmatic-hydrothermal systems range up to 400°C, whereas geothermal fluids at surface are largely <170°C. Magmatic-hydrothermal systems consist of highly reactive liquids whereas geothermal systems are near neutral pH (Giggenbach, 1984, 1997). The difference in reactivity between the two systems is related to the contribution of condensed magmatic volatiles (SO_2, HCl, HF) on one hand, and the degree of wall-rock interaction on the other (Giggenbach, 1992; Hedenquist, 1995). Despite these end-member groupings, there is a spectrum of physical and chemical characteristics that span the range from volcanic fumaroles to vapors discharged from magmatic-hydrothermal systems and in some magmatic arcs there may be a genetic relationship between the magmatic-hydrothermal environment and the near-neutral fluids that develop within the shallow portion of geothermal systems (e.g., a vapor-cored geothermal system; Reyes et al., 1993). Such a genetic affiliation may also apply to the ancient analogues of these end members, the high-sulfidation and intermediate-sulfidation epithermal deposits (see below).

Magmatic-hydrothermal fluids are associated with many active volcanoes and discharge vapors at temperatures from 400 to 80°C (Table 3) near summit craters, adjacent to high-temperature volcanic fumaroles, or on the flank of the volcano. Chemical and isotopic evidence indicate that such fluids originate from condensation of magmatic vapors into meteoric water

(Giggenbach, 1987; Giggenbach et al., 1990; Taran et al., 1992, 1998; Hedenquist et al., 1994b). This process leads to the generation of a reactive liquid that, if sufficiently heated by magmatic vapor, will begin to boil at shallow depth, generating the vapors that were sampled (Table 3). In addition to vapor discharges, magmatic-hydrothermal liquids may reach the surface as hot springs with a pH as low as 1.0 (Hedenquist, 1995). The compositions of some magmatic-hydrothermal vapors lie close to the sulfur-gas buffer at temperatures >300°C, but most compositions are more reduced, although the rock buffer is approached only at temperatures near 100°C (Fig. 3, gray stars). The sulfidation state of these magmatic-hydrothermal systems (Fig. 4 and 5) shows an overall trend from intermediate at 400°C to high at 150°C, but in detail a wide range is observed, from low to high, even very high. This may be intuitively predicted for such reactive fluids because of the likelihood of large variations of water:rock ratio, in some cases on a very local scale. Giggenbach (1992, p. 1936) likens such transient behavior to the movement of a tennis ball between the two players, or major buffers, with the fluid ball getting caught occasionally by the intervening network of mineral buffers.

What happens to the SO_2 and H_2S as the magmatic vapors cool and condense? In some cases we see that SO_2 remains in solution as H_2SO_3 at temperatures <130°C (Southern Bottom field at Mutnovsky, Kamchatka, Table 3). Although thermodynamic calculations are hindered by the nature of the acidic brine at Mutnovsky, Taran et al. (1992) argue that the measurements indicate SO_2 and H_2S remain in equilibrium in solution at temperatures as low as 200°C. The sulfur-gas buffer for aqueous solution is similar to that of vapor, but is shifted due to differences in liquid-vapor distribution coefficients of the two gas species. The dominant process on cooling to temperatures below 350 to 300°C is disproportionation of SO_2 according to the reaction

$$4\ SO_{2(g)} + 4\ H_2O = 4\ H_2SO_{3(aq)} = H_2S_{(aq)} + 3\ H_2SO_{4(aq)} \qquad (8)$$
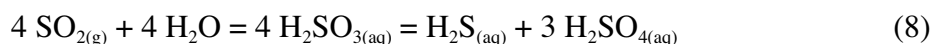
followed by dissociation of H_2SO_4 which yields H^+ ion and ionized aqueous-sulfate species that depend on pH (Fig. 3). Thus, at pH 3 appropriate for reactive magmatic-hydrothermal fluids, the relevant reaction is

$$4\ H_2SO_{3(aq)} = H_2S_{(aq)} + 3\ H_2SO_{4(aq)} = H_2S_{(aq)} + 3\ H^+ + 3HSO_4^- , \qquad (9)$$
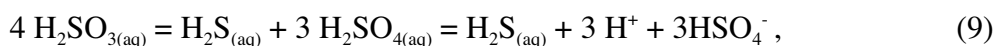
and at pH 6 appropriate for neutral-pH geothermal fluids the reaction is

$$4\ H_2SO_{3(aq)} = H_2S_{(aq)} + 3\ H_2SO_{4(aq)} = H_2S_{(aq)} + 6\ H^+ + 3SO_4^= . \qquad (10)$$

Dissociation of H_2SO_4 allows the buffering capacity of oxidized sulfur species to be consumed by interaction with wall rock, leading to the departure of fluid compositions from the sulfur-gas buffer at these lower temperatures. All of the data for the magmatic hydrothermal systems compiled here plot in the $H_2S_{(aq)}$-predominance field at a pH of 3 (Fig. 3).

Geothermal liquids, in contrast to reactive magmatic-hydrothermal fluids, are closer to equilibrium with their host rock (e.g., Giggenbach, 1981, 1984). These near-neutral pH fluids are relatively reduced (Fig. 3, white stars) and their sulfidation state is typically low to intermediate, near $R_S = 0$ (Figs. 4 and 5) throughout the temperature range 300-100°C. All of the data for the neutral-pH systems plot well into the $H_2S_{(aq)}$-predominance field at a pH of 6 (Fig. 3). The lower (reduced) limit of geothermal compositions has an R_H value of about –3, equivalent to Giggenbach's (1987) rock buffer, which appears to establish a redox "floor", just as the sulfur-gas buffer acts as a redox "ceiling".

These apparent limiting buffer reactions lead to several questions that are relevant to understanding the evolution of ore fluids. If a fluid originates from magma at high temperature in

a state of equilibrium with the sulfur-gas buffer, what controls its evolutionary path as it cools? What is the relative importance of fluid buffers versus mineral and rock buffers, and what is the relative effect of processes such as liquid- and vapor-phase separation? Under what situations is one control more influential than another, and can the relative importance of such controls change in different positions within a hydrothermal system, and/or during its life history?

In order to consider these questions further, we first summarize the typical hydrothermal mineral assemblages of porphyry and epithermal ore deposits (Table 4[1]). In porphyry deposits, hydrothermal assemblages span a wide thermal range, from near-magmatic temperatures to <300°C, similar to the temperature range of volcanic fumaroles. In contrast, epithermal deposits form at temperatures <300°C to as low as 100°C, similar to the lower-temperature end of magmatic-hydrothermal and geothermal systems. We then integrate information on patterns of mineral assemblages in ore deposits with the data from active hydrothermal systems to constrain the space-time evolution and processes of fluid-mineral interaction in ore deposits.

Sulfide Assemblages in Porphyry and Epithermal Deposits

Porphyry copper deposits

The review that follows is limited to porphyry copper deposits associated with medium-K and high-K calc-alkaline magmatic suites in subduction-related continental and oceanic arc environments. We have not included the so-called reduced porphyry Cu-Au deposits of Rowins (2000) because most lack the key features of porphyry-type deposits and many can be classed with gold deposits related to reduced granites (e.g., Thompson and Newberry, 2000). We make brief reference in the next section to porphyry and epithermal ores related to other magmatic suites to point out contrasts with those discussed here.

Data on mineral assemblages and associations, compiled from 30 calc-alkaline porphyry copper deposits, are generalized in Table 4. Note that this table does not achieve the ideals set out above for time-space definition of assemblages. Rather, it lists assemblages as a function of distance from the center of the deposits and generalizes that distal assemblages tend to migrate inward with time and overprint proximal assemblages. Informal "types" (Table 4), likely representing a continuum, have been identified on the basis of the opaque mineral assemblage that dominates the ore zone. Use of assemblages representing the bulk of the ore-grade portions of the deposits focuses the discussion on the dominant ore-depositional environment, but questions remain regarding the possibility that in some deposits erosion has removed high-grade ores of different character. In this context, depth of drilling is unlikely to be an issue, because the majority of these deposits are relatively well-explored by deep drilling.

In Type-1 porphyries most of the high-grade copper ore consists of the assemblage magnetite + bornite + digenite with biotite ± K feldspar (e.g., Batu Hijau, Indonesia; Yerington Mine, Nevada). At the other end of the spectrum, in Type-4 porphyries most of the high-grade ore consists of the assemblage chalcopyrite + pyrite with either biotite + K feldspar or sericite ± chlorite (e.g., Sungun, Iran; Sierrita-Esperanza, Arizona). The majority of the 30 deposits summarized contain magnetite, either as an early phase with or without minor bornite and/or chalcopyrite (19 deposits) or as part of pyrite-absent assemblages containing digenite, bornite,

---

[1] We have not included references in the text for those deposits listed in Table 4 unless we use additional sources for a key observation; sources for deposits not listed in Table 4 are referenced in the text.

and/or chalcopyrite that constitute ore grade (9 deposits). In 19 of the deposits the highest hypogene grades occur in rocks containing the assemblages bornite + magnetite, chalcopyrite + magnetite, or bornite + chalcopyrite, all without pyrite. These deposits are represented by Meyer and Hemley's (1967) "assemblage IV" (Fig. 6). Finally, 12 of the deposits (approximately 30%) contain veins with high and very-high sulfidation state assemblages, and in a small number of these deposits, the high-sulfidation veins represent a significant if not dominant part of the ore (e.g., Collahuasi and Chuquicamata, Chile; Butte, Montana).

In order to plot an average evolutionary path that integrates all packets of fluid for porphyry-copper deposits on diagrams such as Figure 1 we need constraints on temperature as well as sulfidation state. The evidence comes largely from the study of fluid inclusions, but linking a particular fluid inclusion assemblage to the ore-depositional event remains problematic. The bulk of the evidence points to temperatures ranging from 700 to 350°C for K feldspar + biotite assemblages and from 350 to 200°C for chlorite + sericite and quartz + sericite + pyrite (Eastoe, 1978; Preece and Beane, 1982; Reynolds and Beane, 1985; Dilles and Einaudi, 1992; Imai, 2001, Ulrich and Heinrich, 2001). Some recent studies (e.g., Bingham, Utah, Redmond et al., 2001; Bajo de la Alumbrera, Argentina, Ulrich and Heinrich, 2001) show that K feldspar + quartz + biotite ± magnetite formed at 700-400°C, but suggest that most of the chalcopyrite and bornite began to precipitate in equilibrium with this assemblage at 400 to 350°C. Cooler fluids were responsible for pyrite + chalcopyrite ore associated with chlorite + sericite at temperatures of 350°C at Sierrita-Esperanza, 350-275°C at Santa Rita, New Mexico and at Far Southeast, Philippines (Hedenquist et al., 1998), and 310-270°C for sericitic assemblages at Panguna, Papua New Guinea. Based on the above assemblages and temperatures, the environment of porphyry copper ores spans the range from 500°C at low sulfidation states to 270°C at intermediate sulfidation states. The main-line environment for porphyry copper deposits does not cross the reaction chalcopyrite + S_2 = pyrite + bornite (bold arrow, Figs. 1 and 8).

Based on the data presented above, ore deposition at the relatively high temperatures of potassic alteration in porphyry copper deposits took place over a range of sulfidation states from low to intermediate. The ore assemblages of Type-1 and Type-4 porphyries, magnetite + bornite and chalcopyrite + pyrite, respectively, partly overlap in sulfidation and oxidation states, but only magnetite + bornite is stable at low sulfidation states, and chalcopyrite + pyrite is stable into the higher range of intermediate sulfidation states (Figs. 6 and 7). Given the tendency for oxidation and sulfidation state to increase with decreasing temperature, these differences in ore assemblages could reflect higher temperatures of initial copper deposition in Type-1 porphyries than in Type-4 porphyries, or sulfidation of low-grade magnetite + bornite mineralization to chalcopyrite + pyrite ore in Type-4 porphyries. Additionally, differences in the composition of associated igneous rocks (granodiorite-tonalite in Type-1, quartz monzonite-granite in Type-4) could play a role, as shown to be the case by Barton et al. (1995) for porphyry copper deposits in Mexico.

A contrast – very low sulfidation states of some ores related to alkaline magmatism

Sulfide mineral assemblages in many porphyry molybdenum and tungsten deposits associated with highly evolved granites and alkaline magmatic suites (Carten et al., 1993; Jensen and Barton, 2000) are of lower sulfidation state than those associated with the subalkaline porphyry Cu-Au-Mo deposits treated here. Among the better documented molybdenum and tungsten deposits in terms of sulfide assemblages are the Mount Pleasant porphyry W-Mo-(Sn) and Burnthill W deposits, New Brunswick, and the Henderson porphyry Mo deposit, Colorado, all belonging to the high-silica rhyolite-alkalic class of Carten et al. (1993).

At Mount Pleasant the assemblages native bismuth + arsenopyrite ± bismuthinite and loellingite + arsenopyrite (Kooiman et al., 1986) formed at temperatures above 400ºC (Samson, 1990). Lower temperature polymetallic veins at Mount Pleasant contain tin-bearing sulfides, sphalerite, galena, and chalcopyrite, lesser arsenopyrite and loellingite, and minor bornite, tennantite, and pyrite (Kooiman et al., 1986). Note that the assemblage bornite + pyrite is not implied. Burnthill contains native bismuth, loellingite, and pyrrhotite (MacLelland and Taylor, 1989). These New Brunswick deposits, therefore, show a cooling trend from very low sulfidation states, whose upper limit is defined by the reaction loellingite + pyrrhotite + S_2 = arsenopyrite, through low sulfidation states (defined by pyrrhotite + native bismuth), to intermediate sulfidation states at lower temperatures implied by pyrite, tennantite, and chalcopyrite (Fig. 8, arrow labeled "Mt Pleasant").

At Henderson, pyrrhotite, indicative of low sulfidation states, is a minor mineral on the flanks of the Seriate intrusion (Seedorff, 1988), where it formed around 350-400ºC (Fig. 8; arrow labeled "H") and was overprinted by pyrite at 300-350ºC (E. Seedorff, unpublished data, 1987). More widespread and characteristic of Henderson is magnetite ± pyrite, possibly overlapping the porphyry copper deposits in terms of sulfidation state. Thus, Henderson lies at sulfidation states that are intermediate between the relatively lower sulfidation states of the New Brunswick tungsten deposits and the relatively higher sulfidation states of calc-alkalic porphyry-copper deposits. Parallel contrasts are evident in comparing epithermal deposits associated with alkalic igneous rocks with those associated with calc-alkalic igneous rocks. Although alkaline magmas and their hydrothermal fluids are relatively oxidized, sulfide assemblages in related epithermal ores are mostly of intermediate to low sulfidation state (Richards, 1995; Jensen and Barton, 2000; Sillitoe and Hedenquist, this volume).

Porphyry-copper related base-metal vein deposits

Associated with some calc-alkaline porphyry-copper plutons are base-metal deposits in which copper ores of very high- and high sulfidation state occur in veins, massive replacements, and sulfide-cemented breccia bodies. Zoning is generally well-developed, from central enargite-bearing copper ores associated with advanced argillic and/or sericitic alteration to outer tennantite-bearing (Cu)-Pb-Zn ores associated with intermediate argillic alteration (Petersen, 1965; Meyer and Hemley, 1967; Einaudi, 1982; Bartos, 1989; Hemley and Hunt, 1992). Many are superimposed on coeval porphyry-copper deposits and constitute the majority of copper ore (e.g., Main Stage veins at Butte; Rosario and La Grande veins at Collahuasi, Chile; Main Stage veins at Chuquicamata, Chile; see Table 4). Similar copper veins may be spatially separated from their porphyry roots, such as the Magma vein (Hammer and Petersen, 1968) located 2 km north of the recently discovered Magma porphyry copper deposit, Arizona (Manske and Paul, 2002), or may have no known link to mineralized porphyries, such as the copper veins in the volcanic diatreme at Cerro de Pasco, Peru (Graton and Bowditch, 1936; Petersen, 1965; Einaudi, 1977). Sharing many of the features of porphyry-related base-metal veins are the HS epithermal Au-(Cu) deposits with enargite ore in vuggy quartz associated with advanced-argillic alteration (see below).

A common feature of porphyry-related veins is an early stage of sulfidation and silicification of wall rocks accompanied by abundant pyrite as vein fill. This early pyrite-quartz stage is followed by the deposition of Cu-Fe-As-sulfides within veins (e.g., Butte and many others) or in pyrite-matrix intrusive breccias (e.g., Bisbee, Arizona; Bryant, 1968), with or without additional pyrite. With time at a given point, the ore sulfides become increasingly

copper-rich, in the sequence chalcopyrite, bornite, digenite, and the transition in time and space from tennantite to enargite occurs at or near the transition from pyrite + chalcopyrite to pyrite + bornite (e.g., Butte; El Salvador, Chile; Magma vein, Table 4). This latter feature is so common as to constitute evidence that the thermodynamic approximation for reaction 4, tennantite + S_2 = enargite (Craig and Barton, 1973), is one or two log units too low in fS_2, or that the presence of Sb, Fe, and Zn in natural ores stabilizes tennantite relative to enargite. Therefore, we empirically adjusted reaction 4 upward on all figures.

Butte, Montana (Table 4), remains the touchstone against which all porphyry-related veins are compared, in part because this deposit is the giant of its class, but more importantly because of the detailed descriptions of the rocks and ores and the insightful interpretations by Reno Sales and Chuck Meyer. The assemblage pyrite + digenite + covellite is present only in a restricted area of the Central zone that is generally characterized by pyrite, chalcocite, and enargite, with chalcocite the most abundant copper mineral. The Central zone is surrounded by a Transition zone containing pyrite, bornite, chalcopyrite, and tennantite with residual sphalerite, and a Peripheral zone containing Zn, Pb, and Ag sulfides and Mn carbonate. The broad patterns of relative age of sulfides indicate that inner zones encroached on outer zones, as first suggested on the basis of alteration (Sales and Meyer, 1949). For example, residual sphalerite is common in tennantite + chalcopyrite ores of the Transition zone but is mostly replaced in the Central zone. However, there are late reversals of the overall temporal sequence, interpreted by Sales and Meyer (1949) to have taken place on cooling, such as bornite replacing chalcocite and tennantite replacing enargite throughout the Intermediate zone (Meyer et al. 1968), a paragenetic sequence noted in many similar deposits by McKinstry (1963).

Many porphyry-related veins exhibit patterns similar to those at Butte. The Main stage veins at Chuquicamata and the Rosario vein, Collahuasi district, Chile are superimposed on porphyry-style assemblages of intermediate sulfidation state (Table 4). Enargite appears to join the Cu-Fe-sulfides late, and at Chuquicamata sphalerite occupies a high and/or fringe position relative to enargite, analogous to Butte, El Salvador, and Magma. The youngest veins at Chuquicamata and Rosario consist of the very-high sulfidation state assemblage covellite + digenite ± pyrite. Thus, these deposits display the same increasing sulfidation state with time seen at Butte, although zoning relations are less clear at Chuquicamata. A late reversal to lower sulfidation state is recognized at Rosario, where late chalcopyrite replaced chalcocite and digenite, and tennantite replaced enargite (Dick et al., 1994).

Chalcocite appears in some deposits as an important ore mineral in areas where wall rocks were converted to quartz ± pyrophyllite ± dickite, as in the Central zone at Butte and in high-level veins of the Magma porphyry deposit (Manske and Paul, 2002). Chalcocite represents a significant departure from the typically very high- and high-sulfidation states of such areas, being stable only at the transition from intermediate to low sulfidation states at temperatures near 300°C (Figs. 4 and 8). Wide fluctuations in sulfidation states are indicated, and this "anomalous" chalcocite may represent a stage of ore deposition where much of the sulfur and H^+ ion had been consumed and the fluid had returned to its wall-rock buffer due to reaction at depth.

Epithermal gold-silver deposits

Epithermal precious-metal deposits have long been distinguished into two end-members (Table 1), with a distinct difference noted in the associated alteration halo. In high-sulfidation (HS) deposits, the host rock is a leached residue of quartz, commonly vuggy in texture, with a halo of quartz + alunite ± pyrophyllite ± dickite, indicating relatively low pH fluids. In "low-

sulfidation" ("LS") deposits, halos of illite (or chlorite) ± adularia grade out to propylitic alteration, indicating that the pH of the fluid was near neutral. Revision of this classification of epithermal deposits into high-sulfidation, intermediate-sulfidation (IS, formerly "LS") and low-sulfidation (LS) deposits (Table 4) has been suggested recently on the basis of further examination of sulfide assemblages and magmatic-tectonic affiliations (John et al., 1999; Hedenquist et al., 2000; John, 2001; Sillitoe and Hedenquist, this volume). Here we summarize the space-time distribution of sulfide assemblages in these deposits, focusing on variability in sulfidation states within single deposits, among deposits of the same class, and between classes.

In epithermal deposits many of the sulfidation reactions already referred to apply, but the common occurrence of sphalerite in these deposits provides an additional useful measure of sulfidation state. The mole percent FeS in sphalerite coexisting with pyrite or pyrrhotite is continuously variable as a function of sulfidation state (Scott and Barnes, 1971; Czamanske, 1974): 40 to 20 mole percent FeS at low sulfidation states, 20 to 1 at intermediate sulfidation states, 1.0 to 0.05 at high, and <0.05 at very high (Fig. 5). Unfortunately, there are few studies that document sphalerite compositions in any detail and address the question of equilibrium with iron sulfides.

Residual, vuggy quartz, a common but not determining characteristic of HS epithermal deposits, typically contains disseminated pyrite and SiO_2 concentrations >95 wt percent. It forms bodies that flare out upwards and/or preferentially replace a lithologic unit. In many cases, residual quartz lacks base and precious metals and constitutes a barren lithocap of advanced argillic alteration (Sillitoe, 1995). In some cases, barren bodies of advanced argillic alteration overlie porphyry copper deposits, as in the Yerington district, Nevada (Lipske and Dilles, 2000) and El Salvador (Gustafson and Hunt, 1975; Watanabe and Hedenquist, 2001). In other cases, after the leaching stage, copper and gold were introduced to form epithermal Au-(Cu) deposits with abundant sulfides (e.g., Summitville, Colorado, and many others).

There are two typical sequences of mineral deposition in HS epithermal deposits. In one, pyrite + enargite ± luzonite ± famatinite is early, followed by chalcopyrite + pyrite ± tennantite ± sphalerite ± galena. Also post-dating the enargite assemblage is the gold stage, consisting of electrum and gold tellurides, as at Lepanto (Claveria, 2001) as well as Goldfield, Nevada; El Indio, Chile; and Kochbulak, Uzbekistan (Kovalenker et al., 1997). However, at Goldfield electrum appears to predate tennantite, whereas at Lepanto and El Indio electrum post-dates tennantite. In silver-rich deposits of this type, Ag sulfosalts are typically associated with the tennantite ± tetrahedrite zone. At Julcani, Perú, this zone is distal from the central pyrite + enargite assemblage (Deen et al., 1994). In the second sequence, as exemplified by Summitville and La Mexicana, Argentina, there is a transition toward the surface from pyrite + tennantite + chalcopyrite + sphalerite to pyrite + enargite ± luzonite ± sphalerite ± chalcopyrite. At Lahóca, Hungary, tennantite is replaced by enargite, and gold is associated with pyrite relatively late in the sequence, with or after enargite. In both sequences, barite is typically very late and shallow, and can be associated with gold, as at Tambo, Chile (Jannas et al., 1999). Hypogene covellite is rare in these deposits and where it occurs it commonly is the latest sulfide in vugs prior to filling by native sulfur, as at Nansatsu, Japan (Hedenquist et al., 1994a). Thus, covellite in HS epithermal deposits occupies the same temporal position as it does in many porphyry-related base-metal vein deposits. There is a wide range of FeS content in sphalerite in HS epithermal deposits (e.g., 0.02 to 7 mole percent at La Mexicana) suggesting a wide range of sulfidation states from intermediate to very high (Fig. 5).

Based on the above summary, the sulfidation state in HS epithermal deposits ranged from high for the enargite assemblage to intermediate for the tennantite-tetrahedrite + pyrite ± chalcopyrite assemblage (Fig. 4). At Goldfield, Lepanto and Julcani, high sulfidation states evolved to intermediate sulfidation states with time and/or distance from source. At Summitville, La Mexicana, and Lahóca, the opposite was the case: intermediate sulfidation states evolved to high sulfidation states at more shallow depths or with time. In some deposits, very high sulfidation states were achieved at very shallow levels, but the timing relative to other assemblages is not clear.

IS epithermal deposits that are also sulfide-rich share many of the sulfide assemblages of HS deposits, except that the enargite-bearing assemblage is lacking (Table 4) and the Ag:Au ratios are higher, at least 10:1, and typically >100:1. The total sulfide content can be highly variable, from 1 to > 10 percent (Albinson et al., 2001). These features are characteristic of the base-metal + silver veins of Mexico (Pachuca, Fresnillo), USA (Comstock Lode, Nevada; Creede, Colorado), Perú, Romania and elsewhere. The veins have a halo of illite ± adularia which grades downward to sericitic and outward to propylitic assemblages. The major sulfide assemblage can be relatively simple, including combinations of sphalerite, galena, pyrite, chalcopyrite, and tetrahedrite. Silver is present as Ag sulfosalts, and in some cases a large variety of these minerals occur in trace quantities, either relatively late in the sequence (Pachuca) or down the flow path (Creede). Sphalerite compositions range from <1 to 10 mole percent FeS, locally up to 20 mole percent FeS (e.g., Creede; Barton et al., 1977), covering the full range of intermediate sulfidation states (Fig. 5) but consistent with the assemblage pyrite + chalcopyrite + tetrahedrite/tennantite (Fig. 4). Such fluctuations in the FeS content of sphalerite may be caused by intermittent events such as boiling, local wall rock interaction, or by pulses of reduced fluids of magmatic or sedimentary origin (Barton et al., 1977; Bethke and Rye, 1979).

A third class of epithermal deposit, the low sulfidation (LS) deposits, are found in association with both subalkalic (including bi-modal thoeleiitic + calc-alkalic) and alkalic igneous rocks. Here we focus on deposits related to subalkaline magmatic provinces (Table 4) rather than alkaline (Jensen and Barton, 2000; Sillitoe and Hedenquist, this volume). Subalkalic LS epithermal deposits are sulfide-poor, dominated by gold typically of bonanza grades, and can be distinguished from HS and IS deposits on the basis of the ore-mineral assemblage (John et al., 1999; Hedenquist et al., 2000; John, 2001). Alteration halos are narrow and consist of illite or chlorite, with chlorite dominant in more mafic host rocks. These deposits appear to form at relatively low temperature (< 220°C) and at shallow depths (< 250 m), in places immediately beneath hot spring sinters, as at McLaughlin, California (Sherlock et al., 1995). The very low sulfide content, <1 volume percent, is dominated by pyrite (in some cases with arsenian rims), although marcasite also is common as a result of low temperatures. Gold as electrum, in places dendritic (Saunders, 1994), is closely associated with naumannite (Ag_2Se) (e.g., ginguro or black ore at Hishikari and other bonanza deposits in Japan) or pyrite (Sleeper and Midas, Nevada) and is typically present in bands of botryoidal quartz or chalcedony. Other sulfides are present only in trace amounts, and include sphalerite, chalcopyrite, galena, Ag sulfosalts, and minor occurrences of arsenopyrite and rare pyrrhotite as at Esquel, Argentina; Mule Canyon, Nevada; Rio Blanco, Ecuador; and El Limon, Nicaragua (Sillitoe, 2002; John et al., 1999; J. Sutcliffe, pers. commun., 2002; M. Gareau, pers. commun., 2002). Within the gold ore-zone the total base-metal content is typically less than a few 100s ppm. Analyses of sphalerite from two Nevada deposits indicate a range from 1 to 15 mole percent FeS (John, 2001). Mercury, As and Sb can be highly anomalous due to the low temperature and shallow depth of formation, and orpiment,

realgar and stibnite are common minerals, typically late. At 200°C, orpiment is stable at high sulfidation states and realgar at intermediate sulfidation states (Fig. 4), higher by several log units fS_2 than the low sulfidation states implied by arsenopyrite and pyrrhotite.

Discussion and Conclusions

Sulfidation state, referenced to stability fields of sulfide mineral assemblages as a function of log fS_2 and temperature, has been used to define Main Line ore-forming environments and to identify evolutionary trends in individual deposits, supported by the many examples cited here. However, this indicator, with rare exceptions (e.g., Barton et al., 1995), has seen little use in comparisons between or within deposit types. Here we suggest that sulfidation state (and its companion, oxidation state), in combination with R_S and R_H, can offer significant insight into the commonality of fluid evolution between active and extinct hydrothermal systems, as well as underscore distinctions and similarities between different classes of intrusion-centered deposits.

Looping path of porphyry-copper and related base-metal vein deposits

At the deeper and hotter levels of the porphyry environment, mineral assemblages are consistent with the fluid closely following the sulfur-gas buffer during cooling to temperatures of 500 to 400 °C, with this gas-buffered path causing pronounced increases in sulfidation and oxidation states. The high-temperature volcanic fumaroles, our proxies for the higher-temperature portion of the porphyry environment, plot largely in the bornite + magnetite and chalcopyrite + magnetite fields (Fig. 7), consistent with the view that assemblages in porphyry copper deposits are derived through exsolution and cooling of magmatic volatiles. The general environment for porphyry copper deposits (gray arrow, Fig. 8) is variably modified by excursions that result from such opposite extremes as mixing with magmatic SO_2-bearing gases in major fissures (white arrow "O", Fig. 8) or approaching the rock buffer in distal fractures (white arrow "N", Fig. 8).

Sulfide assemblages in central portions of porphyry-related vein deposits represent the peak in the trend toward increasing sulfidation state that we see in the porphyries. Mineral reaction curves sweep to higher X_{H_2} / X_{H_2S} (R_S) values with declining temperature as the fluid path sweeps to lower R_S (Figs. 5 and 8), resulting in marked zonal and/or temporal changes in Cu-Fe-As-S mineral assemblages that commonly are difficult to interpret. Hydrothermal fluids in these deposits achieve their lowest value of $R_S = -3$ (highest sulfidation state, approximately equal to digenite $+S_2$ = covellite) at temperatures near 300°C (arrow labeled "T" on Fig. 8). This peak of reactivity results from cooling-induced generation of H^+ (reactions 9 or 10) outrunning the consumption of H^+ through hydrolysis reactions with fresh wall-rocks (Meyer and Hemley, 1967). Reactivity is enhanced by boiling (Reed, 1997) and/or by addition of new SO_2 from a degassing magma chamber at depth (Brimhall, 1979, 1980; arrow labeled "SO_2 flux", Fig. 8). The path will be accentuated further if fluids are isolated from their rock buffer, a more likely case in vein deposits than in fracture-controlled porphyry-type deposits. Thus, Sales and Meyer (1949) concluded that high sulfidation states were achieved in the Central Zone at Butte because fluids were restricted to fissures with sericite-pyrite walls. The same conclusion can be applied to the early pyrite + enargite assemblage typical of residual quartz in HS epithermal deposits. In the absence of wall rocks leached during earlier hydrothermal activity, acidic ore fluids characteristic of very high sulfidation states are unlikely to develop.

From this peak in reactivity, the sulfidation state eventually declines as equilibrium with fresh wall rock is achieved and as sulfur is lost from solution. The "isothermal looping path" shown in Figure 6 "can therefore also be construed as the trace of a more gently curved path of decreasing hydrothermal temperature" (Meyer and Hemley, 1967, p. 232), the Lazy-L pattern shown in Figures 1, 2, and 8.

Looping path of active magmatic hydrothermal systems

The composite pattern of all volcanic fumaroles and active magmatic-hydrothermal samples (Figs. 3, 4, and 5) mimics the looping path defined by porphyry-copper related ores, although it is shifted to lower temperatures. In the active systems the trend toward higher sulfidation and oxidation states on cooling is reversed at around 100-130ºC. The clearest example of this reversal in R_H and R_S comes from White Island (Figs. 4 and 5), where five samples were collected from 760 to 100°C fumaroles on a north-south traverse on the same day in February, 1984 (Giggenbach, 1987). The 100°C sample has the lowest R_{SH} (X_{SO_2} / X_{H_2S}) value (Table 3), indicating that SO_2 has to a large extent been reduced to H_2S through wall-rock interaction, causing an increase in R_H relative to other low-temperature samples. A similar pattern is suggested by the data from Vulcano (Fig. 5), although samples at temperatures between 300 and 100 °C are absent. The minimum R_H and R_S values for active fluids are near 115ºC whereas in porphyry-copper related deposits these minima are near 300ºC. This difference is an artifact of surface sampling because a vapor separated from a 250-300ºC liquid at depth will reach the surface at a maximum temperature of 171ºC, a function of the enthalpy of the liquid (White et al., 1971). Most of the vapors generated from such fluids cool even more and reach the surface at <130ºC. Therefore, a fundamental difference in actual reversal temperatures between modern and ancient systems is unlikely.

HS deposits – variations on the theme of porphyry-related base-metal veins

HS epithermal Au-(Cu) deposits with enargite in residual quartz (e.g., Lepanto, La Mexicana, Lahóca; Table 4) have many similarities to porphyry-related base-metal deposits. These similarities extend beyond their common association with porphyry copper deposits, and include structural style, ore textures, wall-rock alteration, and sulfidation states reflected in their mineral assemblages. Many HS deposits hosted by residual quartz show a shift to lower sulfidation states with time (Fig. 8), with enargite replaced by tennantite at the time of gold deposition. In common with porphyry-related base-metal veins, this decline in sulfidation state is likely because the enargite stage is far from equilibrium with wall rock outside the silicic host, and the natural long-term tendency is for hydrothermal fluids to become reduced.

Differences between these two classes of deposits also are evident. Porphyry-related base-metal veins typically are well zoned, whereas HS deposits are highly telescoped, suggesting that the latter deposits formed at shallower depths in environments with steep thermal gradients. Base-metal veins have a more complex mineralogy and metal suite that includes copper, zinc, lead, and silver, and they tend to be associated with molybdenum-bearing, gold-poor porphyries. In contrast, many HS epithermal Au-(Cu) deposits are associated with gold-rich porphyry copper districts with minor molybdenum and other metals (cf., Barton et al., 1995).

HS epithermal deposits – affiliation with IS deposits

The gold-bearing sulfide assemblages of the HS epithermal deposits are similar to those of IS deposits. IS veins are common on the margins of HS deposits (Sillitoe, 1999; Sillitoe and Hedenquist, this volume); at Lepanto and Victoria, Philippines, these two styles of deposit are

closely related in both time and space (Claveria, 2001), although Victoria may be about 0.2 m.y. younger. Indeed there may be some affiliation between HS and IS epithermal deposits, as suggested by Reed (1997) on theoretical grounds, with differences in metal proportions (Cu-Au versus Pb-Zn-Ag-Au, respectively) likely resulting from progressive, wall-rock induced reduction and neutralization of reactive fluids, a process that affects concentrations of HCl, SO_2 and H_2S and consequently constrains metal concentrations in the fluid. A transition from HS to IS epithermal deposits would be analogous to the transition commonly seen in porphyry copper districts from proximal copper-dominated ores to distal lead-zinc-silver ores (Table 4).

Arc magmas and battle of the buffers

As noted earlier, the oxidation state of hydrothermal fluids from active systems associated with andesitic arc magmas plot within the envelope established by the sulfur-gas buffer and the rock buffer (Fig. 3). These two buffers overlap at magmatic temperatures, as gas species appear to be in equilibrium with andesitic magma, but they diverge to 3 units of R_H difference at 300 °C. Thus, a condensed magmatic fluid will become progressively more reactive relative to typical fresh host-rocks as the temperature decreases.

In contrast to volcanic fumarole compositions, where redox states are controlled by the sulfur-gas buffer, most vapor compositions related to lower temperature acidic magmatic-hydrothermal and near-neutral pH geothermal systems plot below the respective $H_2S_{(aq)} = HSO_4^-$ (pH 3) and $H_2S_{(aq)} = SO_4^=$ (pH 6) predominance boundaries (Giggenbach, 1997) within the $H_2S_{(aq)}$ field (Fig. 3), suggesting an absence of buffering by aqueous-sulfur redox equilibria at epithermal temperatures as concluded by Barton et al. (1977) for Creede. It is clear from Figure 3 that individual mineral buffers also do not match the fluid patterns.

Examination of fluid compositions in active systems on R_H and R_S diagrams (Figs. 3 and 5) highlights several features relevant to the above summary. High-temperature volcanic vapors have a linear trend that reflects the correlation between R_H (X SO_2 / X H_2O) and R_{SH} (X SO_2 / X H_2S). Measured values of X SO_2 / X H_2S of about 1 to 10, (or R_{SH} of 0 to 1; Table 3) agree with the ratio predicted from X SO_2 / X H_2O. From their high-temperature magmatic origins, the cooling path of sampled magmatic-hydrothermal fluids from numerous individual localities (Table 3; tie-lines on Figs. 3 and 5) evolve to lower R_H and R_S values (higher oxidation and sulfidation states). This evolutionary trend may be a consequence of SO_2 and H_2S gases dominating other redox gases (e.g., CH_4 or H_2; Table 3). Where $SO_2 \approx H_2S$, the disproportionation reaction (equations 8, 9 and 10) will lead to fluids having relatively high oxidation and sulfidation states. Boiling may be important in some cases because it will result in progressive oxidation of the residual liquid due to loss of H_2 to the vapor phase. If the boiling liquid is H_2S-dominant, then the sulfidation state also will increase with a slope parallel to the boiling trend shown in Figure 5 (Appendix). Divergence from the gas buffer begins at 400ºC, where SO_2 declines significantly, and below 300ºC SO_2 gas joins S_2 gas as a negligible species for all reasonable hydrothermal environments. At these lower temperatures, H_2 and H_2S remain the dominant gases, and near the rock buffer $H_2 = H_2S$ ($R_S = 0$), typical of geothermal fluids (Table 3) and LS epithermal gold deposits.

Reduced geothermal systems and subalkalic LS epithermal deposits

In contrast with the acidic fluids of magmatic-hydrothermal systems, the near-neutral pH fluids from geothermal systems have generally lower sulfidation and oxidation states at 300-200°C, but overlap with the magmatic-hydrothermal fluids at 100°C near the rock buffer. As

suggested by the R_H and R_S diagrams (Figs. 4 and 5), the 300-200°C geothermal samples are all stable with respect to pyrite + magnetite, but lie close to the pyrrhotite field, consistent with the mineral assemblages in subalkalic LS epithermal deposits. Perhaps these LS deposits reflect a greater degree of water:rock interaction, or form from fluids with a smaller magmatic component. Alternatively, for some LS deposits hydrothermal fluids may be related to reduced tholeiitic magmas in rift settings (John, 2001) (Figs. 2B and 3). In reduced hydrothermal systems, simple cooling, even accentuated by boiling, is unlikely to result in any appreciable increase in sulfidation state. We interpret the geothermal fluids compiled in this paper to be analogs both for IS epithermal deposits and for subalkalic LS epithermal Au deposits of extensional arcs (e.g., Bodie, California; Hishikari, Japan: see Sillitoe and Hedenquist, this volume).

Concluding remarks

Variability of sulfidation and oxidation states of ore assemblages is a ubiquitous feature in the ore deposits considered here. This variability is a complex function of thermally prograding and retrograding hydrothermal episodes, and of intermittent events such as boiling, local wall rock interaction, or input of new hydrothermal fluids of magmatic or non-magmatic origin, all taking place as hydrothermal conduits shift location. On considering the complexities of sulfide assemblages at Butte, Sales and Meyer (1949) concluded that "the fact that a recognizably systematic district-wise pattern of mineralization and alteration has emerged is more surprising than the fact that there are frequent local divergences from that pattern" (p. 467). They conclude that microtextures between minerals are commonly ambiguous, and can only be interpreted within the context of the deposit-scale mineral-distribution patterns.

Considering individual epithermal deposits, local divergence of sulfidation state from the norm can lead to apparent inconsistencies with the overall classification into HS, IS and LS types. Although there may be problems with the classification scheme, as there are with many others, we stress that the classification terms highlight only one aspect (the sulfide mineral assemblage) of the combination of features, including magmatic, tectonic, hydrothermal, and geochemical, that should be used in classifying. Importantly, though, variability of sulfidation state within deposits blurs distinctions, suggests continua between deposit types, and indicates that common processes are active in different deposit types.

Regarding continua in terms of evolutionary paths, the sulfidation and redox environments of deposits discussed in this paper show a bimodal spectrum consisting of, on the one hand, oxidized porphyry copper and related base-metal veins and HS epithermal deposits, possibly including an affiliation with IS epithermal deposits down the flow path, and, on the other hand, relatively reduced LS epithermal gold deposits. A bimodal spectrum is also seen in active hydrothermal systems, with the first represented by fumaroles and magmatic-hydrothermal fluids associated with andesitic arc magmas, and the second represented by the neutral-pH geothermal systems.

The tendency for oxidized magmas to be associated with high-sulfidation deposits and for reduced magmas to be associated with low-sulfidation deposits is seen in the contrast between andesitic arc-related IS deposits and bimodal rift-related LS deposits in the western U. S. (John, 2001). However, there are many exceptions, including the relatively oxidized alkaline igneous rocks associated with deposits characterized by low to intermediate sulfidation states (Richards, 1995; Jensen and Barton, 2000). Differences among intrusion-related deposits is in part a consequence of the degassing of magmas that have different initial redox-volatile compositions,

but changes in these initial compositions due to loss of sulfur to the near-surface environment, seawater influx, or effects of local wall rocks are likely to blur the distinctions in many cases.

Samples from different portions of an active hydrothermal system provide information on the spatial evolution of fluids and the processes that influence fluid composition. The data on measured fluid compositions represent a single time frame in the life history of a given system, ranging from a single day of sampling (e.g., White Island, New Zealand; Giggenbach, 1987) to at most a half century of monitoring. By contrast, information from ore deposits provides an indication of the temporal and spatial evolution of hydrothermal systems that encompass a lifetime of several 10 thousand to a few 100 thousand years, although the link between time and space continues to be elusive in most districts. In this context, we note that samples from a variety of individual active systems span the whole time-space range seen in individual ore deposits of porphyry affiliation, reinforcing the concept of contemporaneous zonal growth proposed by Reno Sales and Charles Meyer.

Acknowledgements

References

Albinson, T., Norman, D. I., Cole, D., and Chomiak, B., 2001, Controls on formation of low-sulfidation epithermal deposits in Mexico: Constraints from fluid inclusion and stable isotope data, *in* Albinson, T. and Nelson, C.E., eds., New mines and discoveries in Mexico and Central America: Society of Economic Geologist Special Publication 8, p. 1-32.

Allard, P., 1983, The origin of hydrogen, carbon, sulphur, nitrogen and rare gases in volcanic exhalations: evidence from isotope geochemistry, *in* Tazieff, H., and Sabroux, J-C., eds., Forecasting volcanic events: Amsterdam, Elsevier Science Publishing Co., p. 337-386.

Andersen, D. J., Bishop, F. C., and Lindsley, D. H., 1991, Internally consistent solution models for Fe-Mg-Mn-Ti oxides; Fe-Mg-Ti oxides and olivine: American Mineralogist, v. 76, p. 427-444.

Andersen, D. J., Lindsley, D. H., and Davidson, P. M., 1993, QUILF; a Pascal program to assess equilibria among Fe-Mg-Mn-Ti oxides, pyroxenes, olivine, and quartz: Computers & Geosciences, v. 19, p. 1333-1350.

Barnes, H. L., and Czamanske, G. K., 1967, Solubilities and transport of ore minerals, *in* Barnes, H. L., ed., Geochemistry of hydrothermal ore deposits: New York, Holt, Rinehart and Winston, p. 334-381.

Barnes, H. L., and Kullerud, G., 1961, Equilibria in sulfur-containing aqueous solutions in the system Fe-S-O, and their correlation during ore deposition: Economic Geology, v. 56, p. 648-688.

Barton, M. D., 1996, Granitic magmatism and metallogeny of southwestern North America: Transactions of the Royal Society of Edinburgh: Earth Sciences, v. 87, p. 261-280.

Barton, M. D., Staude, J. M. G., Zurcher, L., and Megaw, P. K. M., 1995, Porphyry copper and other intrusion-related mineralization in Mexico, *in* Pierce, F. W., and Bolm, J.G., eds., Porphyry copper deposits of the American cordillera: Arizona Geological Society Digest 20, 486-524.

Barton, P. B., Jr., 1970, Sulfide petrology: Mineralogical Society of America, Special Paper No. 3, p. 187-198.

Barton, P. B., Jr., and Skinner, B. J., 1967, Sulfide mineral stabilities, *in* Barnes, H. L., ed., Geochemistry of hydrothermal ore deposits: New York, Holt, Rinehart and Winston, p. 236-333.

Barton, P. B., Jr., and Skinner, B. J., 1979, Sulfide mineral stabilities, *in* Barnes, H. L., ed., Geochemistry of hydrothermal ore deposits, Second Edition: New York, Holt, John Wiley & Sons, p. 278-403.

Barton, P. B., Jr, Toulmin, P., III, and Sims, P. K., 1960, Role of chemical potential of sulfur in controlling mineral assemblages in sulfide deposits: Economic Geology, v. 55, p. 1336.

Barton, P. B., Jr., Bethke, P. M., and Toulmin, P., III, 1963, Equilibrium in ore deposits: Symposium on the mineralogy of sulfides--International Mineralogical Association, 3rd General Meeting, Washington, DC, 1963, p. 171-185.

Barton, P. B., Jr., Bethke, P. M., and Roedder, E., 1977, Environment of ore deposition in the Creede mining district, San Juan Mountains, Colorado: Part III. Progress toward interpretation of the chemistry of the ore-forming environment: Economic Geology, v. 72, p. 1-24.

Bartos, P. J., 1989, Prograde and retrograde base metal lode deposits and their relationship to underlying porphyry copper deposits: Economic Geology, v. 84, p. 1671-1683.

Bethke, P. M., 1984, Controls on base and precious metal mineralization in deeper epithermal environments, U.S.G.S Open File Report 84-0890, 39 p.

Bethke, P. M., and Rye, R. O., 1979, Environment of ore deposition in the Creede mining district, San Juan Mountains, Colorado; Part IV, Source of fluids, from oxygen, hydrogen, and carbon isotope studies: Economic Geology, v. 74, p. 1832-1851.

Borrock, D., Kesler, S. E., and Vogel, T. A., 1999, Sulfide minerals in intrusive and volcanic rocks of the Bingham-Park City belt, Utah: Economic Geology, v. 94, p. 1213-1230.

Bowen, N. L., 1933, The broader story of magmatic differentiation, briefly told, *in* Ore deposits of the Western States (Lindgren volume), American Institute of Mining and Metallurgical Engineers, p. 106-128.

Brimhall, G. H., Jr., 1979, Lithologic determination of mass transfer mechanisms of multiple-stage porphyry copper mineralization at Butte, Montana: Vein formation by hypogene leaching and enrichment of potassium-silicate protore: Economic Geology, v. 74, p. 558-589.

Brimhall, G. H., Jr., 1980, Deep hypogene oxidation of porphyry copper potassium-silicate protore at Butte, Montana: A theoretical evaluation of the copper remobilization hypothesis: Economic Geology, v. 75, p. 384-409.

Bryant, D. G., 1968, Intrusive breccias associated with ore, Warren (Bisbee) mining district, Arizona: Economic Geology, v. 63, p. 1-12.

Buddington, A. F., and Lindsley, D. H., 1964, Iron titanium oxide minerals and synthetic equivalents: Journal of Petrology, v. 5, p. 310-357.

Burnham, C. W., 1979, Magmas and hydrothermal fluids, *in* Barnes, H. L., ed., Geochemistry of hydrothermal ore deposits, 2nd Edition: New York, John Wiley & Sons, p. 71-136.

Burnham, C. W., and Ohmoto, H., 1980, Late-stage processes of felsic magmatism: Mining Geology Special Issue, v. 8, p. 1-11.

Candela, P. A., 1992, Controls on ore metal ratios in granite-related ore deposits: an experimental and computational approach: Transactions of the Royal Society of Edinburgh: Earth Sciences, v. 83, p. 317-326.

Carmichael, I. S. E., and Ghiorso, M. S., 1986, Oxidation-reduction relations in basic magma: a case for homogeneous equilibria: Earth and Planetary Science Letters, v. 78, p. 200-210.

Carson, D. J. T., and Jambor, J. L., 1976, Morrison: Geology and evolution of a bisected annular porphyry copper deposit, *in* Sutherland Brown, A., ed., Porphyry deposits of the Canadian Cordillera, Special Volume 15, Canadian Institute of Mining and Metallurgy, p. 264-273.

Carten, R. B., 1986, Sodium-calcium metasomatism--chemical, temporal, and spatial relationships at the Yerington, Nevada, porphyry copper deposit: Economic Geology, v. 81, p. 1495-1519.

Carten, R. B., White, W. H., and Stein, H. J., 1993, High-grade granite-related molybdenum systems; classification and origin, *in* Kirkham, R. V. e. a., ed., Mineral deposit modeling, 40, Geological Association of Canada, Special Paper, p. 521-554.

Chiodini, G., Cioni, R., Marini, L., and Panichi, C., 1995, Origin of the fumarolic fluids of Vulcano Island, Italy and implications for volcanic surveillance: Bulletin of Volcanology, v. 57, p. 99-110.

Clark, A. H., Archibald, D. A., Lee, A. W., Farrar, E., and Hidgson, C. J., 1998, Laser probe ^{40}Ar/^{39}Ar ages of early- and late-stage alteration assemblages, Rosario porphyry copper-molybdenum deposit, Collahuasi district, I Region, Chile: Economic Geology, v. 93, p. 326-337.

Claveria, R. J. R., 2001, Mineral paragenesis of the Lepanto copper and gold and the Victoria gold deposits, Mankayan mineral district, Philippines: Resource Geology, v. 51, p. 97-106.

Clode, C., Proffett, J. M., Mitchell, P., and Munajat, I., 1999, Relationships of intrusion, wall rock alteration and mineralization in the Batu Hijau copper-gold porphyry deposit: PACRIM '99 Proceedings, Bali, Indonesia, 1999, p. 485-498.

Core, D. P., Kesler, S. E., and Essene, E. J., 2001, Oxygen fugacity and sulfur speciation in felsic intrusive rocks from the Wasatch and Oquirrh Ranges, Utah: Eleventh annual V. M. Goldschmidt Conference, 20-24 May 2001, Hot Springs, Virginia, USA: Abstract 3455, Lunar and Planetary Institute, Houston (CD-ROM).

Cornejo, P. C., and Mahood, G. A., 1997, Seeing past the effects of re-equilibration to reconstruct magmatic gradients in plutons: La Gloria Pluton, central Chilean Andes: Contributions to Mineralogy and Petrology, v. 127, p. 159-175.

Craig, J. R., and Barton, P. B., Jr, 1973, Thermochemical approximations for sulfosalts: Economic Geology, v. 68, p. 493-506.

Czamanske, G. K., 1974, The FeS content of sphalerite along the chalcopyrite-pyrite-bornite sulfur fugacity buffer: Economic Geology, v. 69, p. 1328-1334.

Deen, J. A., Rye, R. O., Munoz, J. L., and Drexler, J. W., 1994, The magmatic hydrothermal system at Julcani, Peru: Evidence from fluid inclusions and hydrogen and oxygen isotopes: Economic Geology, v. 89, p. 1924-1938.

Dick, L. A., Chavez, W. X., Jr., Gonzales, A., and Bisso, C., 1994, Geologic setting and mineralogy of the Cu-Ag-(As) Rosario vein system, Collahuasi district, Chile: SEG Newsletter, Society of Economic Geologists, p. 1.

Dilles, J. H., 1987, Petrology of the Yerington batholith, Nevada: Evidence for evolution of porphyry copper ore fluids: Economic Geology, v. 82, p. 1750-1789.

Dilles, J. H., and Einaudi, M. T., 1992, Wall-rock alteration and hydrothermal flow paths about the Ann Mason porphyry copper deposit, Nevada; a 6-km vertical reconstruction: Economic Geology, v. 87, p. 1963-2001.

Dilles, J. H., Einaudi, M. T., Proffett, J. M., Jr., and Barton, M. D., 2000, Overview of the Yerington porphyry copper district: magmatic to nonmagmatic sources of hydrothermal fluids, their flow paths and alteration effects on rocks and Cu-Mo-Fe-Au ores, *in* Dilles, J. D., Barton, M. D., Johnson, D. A., Proffett, J. M., and Einaudi, M. T., eds., Contrasting styles of intrusion-associated hydrothermal systems, Guidebook Series v. 32, Society of Economic Geologists, p. 55-66.

Drexler, J. W., and Munoz, J. L., 1988, Highly oxidized, pyrrhotite-anhydrite-bearing silicic magmas from the Julcani Ag-Cu-Bi-Pb-Au-W district, Peru; physicochemical conditions of a productive magma, *in* Taylor, R. P., and Strong, D. F., eds., Recent advances in the geology of granite-related mineral deposits, 39: Halifax, Canadian Institute of Mining and Metallurgy - Special Volume, p. 72-79.

Eastoe, C. J., 1978, A fluid inclusion study of the Panguna porphyry copper deposit, Bougainville, Papua New Guinea: Economic Geology, v. 73, p. 721-748.

Einaudi, M. T., 1977, Environment of ore deposition at Cerro de Pasco, Peru: Economic Geology, v. 72, p. 893-924.

Einaudi, M. T., 1982, Description of skarns associated with porphyry copper plutons, southwestern North America, *in* Titley, S. R., ed., Advances in geology of the porphyry copper deposits, southwestern North America: Tucson, AZ, University of Arizona Press, p. 139-184.

Einaudi, M. T., Meinert, L. D., and Newberry, R. J., 1981, Skarn deposits, 75th Anniversary Volume - 1905-1980, Economic Geology, p. 317-391.

Fenner, C. N., 1933, Pneumatolytic processes in the formation of minerals and ores, *in* Ore deposits of the Western States (Lindgren volume), American Institute of Mining and Metallurgical Engineers, p. 58-106.

Fournelle, J., 1990, Anhydrite in Nevado del Ruiz November 1985 pumice: relevance to the sulfur problem: Journal of Volcanology and Geothermal Research, v. 42, p. 189-201.

Fudali, R. F., 1965, Oxygen fugacities of basaltic and andesitic magmas: Geochimica et Cosmochimica Acta, v. 29, p. 1063-1075.

Gatter, I., Molnar, F., Foldessy, J., Zelenka, T., Kiss, J., and Szebenyi, G., 1999, High-and low-sulfidation epithermal mineralization of the Marta Mountains, Northeast Hungary, *in* Molnar, F., Lexa, J., and Hedenquist, J. W., eds., Epithermal mineralization of the western Carpathians, 31, Society of Economic Geologists, Guidebook Series, p. 155-179.

Gemmell, J. B., Simmons, S. F., and Zantop, H., 1988, The Santo Niño silver-lead-zinc vein, Fresnillo, Zacatecas, Mexico: Part I. Structure, vein stratigraphy, and mineralogy: Economic Geology, v. 83, p. 1597-1618.

Geyne, A. R., Fries, C., Jr., Segerstrom, K., Black, R. F., and Wilson, I. F., 1963, Geology and mineral deposits of the Pachuca-Real del Monte district, State of Hidalgo, Mexico: Consejo de Recursos Naturales No Renovables, Publication 5E, 203 p.

Gibbins, S. L., 2000, Alteration in the southwest wall rocks of the Grasberg Cu-Au porphyry deposit: unpub. M.S. thesis, The University of Arizona, 140 p.

Giggenbach, W. F., 1980, Geothermal gas equilibria: Geochimica et Cosmochimica Acta, v. 44, p. 2021-2032.

Giggenbach, W. F., 1981, Geothermal mineral equilibria: Cosmochimica et Cosmochimica Acta, v. 45, p. 393-410.

Giggenbach, W. F., 1984, Mass transfer in hydrothermal alteration systems: Geochimica et Cosmochimica Acta, v. 54, p. 2051-2058.

Giggenbach, W. F., 1987, Redox processes governing the chemistry of fumarolic gas discharges from White Island, New Zealand: Applied Geochemistry, v. 2, p. 143-161.

Giggenbach, W.F., 1992, Magma degassing and mineral deposition in hydrothermal systems along convergent plate boundaries, Economic Geology, v. 87, p. 1927-1944.

Giggenbach, W. F., 1995, Variations in the chemical and isotopic composition of fluids discharged from the Taupo volcanic zone, New Zealand: Journal of Volcanology and Geothermal Research, v. 68, p. 89-116.

Giggenbach, W. F., 1996, Chemical composition of volcanic gases, *in* Scarpa, R., and Tilling, R. I., eds., Monitoring and mitigation of volcano hazards: Berlin, Springer-Verlag, p. 221-256.

Giggenbach, W. F., 1997, The origin and evolution of fluids in magmatic-hydrothermal systems, *in* Barnes, H. L., ed., Geochemistry of hydrothermal ore deposits, Third Edition: New York, John Wiley & Sons, p. 737-796.

Giggenbach, W. F., and Le Guern, F., 1976, The chemistry of magmatic gases from Erta'Ale, Ethiopia: Geochimica et Cosmochimica Acta, v. 40, p. 25-30.

Giggenbach, W. F., Martini, M., and Corazza, E., 1986, The effects of hydrothermal processes on the chemistry of some recent volcanic gas discharges: Periodico di Mineralogia, v. 55, p. 15-28.

Giggenbach, W. F., Garcia, N., Londoño C., A., Rodriguez V., L., Rojas G., N., and Calvache V., M. L., 1990, The chemistry of fumarolic vapor and thermal-spring discharges from the Nevado del Ruiz volcanic-magmatic-hydrothermal system, Colombia: Journal of volcanology and geothermal research, v. 42, p. 13-39.

Giggenbach, W. F., and Matsuo, S., 1991, Evaluation of results from second and third IAVCEI field workshops on volcanic gases, Mt. Usu, Japan, and White Island, New Zealand: Applied Geochemistry, v. 6, p. 125-141.

Graton, L. C., and Bowditch, S. I., 1936, Alkaline and acid solutions in hypogene zoning at Cerro de Pasco: Economic Geology, v. 31, p. 651-698.

Graybeal, F. T., 1982, Geology of the El Tiro area, Silver Bell mining district, Arizona, *in* Titley, S. R., ed., Advances in geology of the porphyry copper deposits, southwestern North America: Tucson, University of Arizona Press, p. 487-505.

Gustafson, L.B., 1963, Phase equilibria in the system Cu-Fe-As-S: Economic Geology, v. 58, p. 667-701.

Gustafson, L. B., and Hunt, J. P., 1975, The porphyry copper deposit at El Salvador, Chile: Economic Geology, v. 70, p. 857-912.

Haggerty, S. E., 1976, Opaque mineral oxides in terrestrial igneous rocks, *in* Rumble, D., III, ed., Oxide Minerals. Short course notes, v. 3: Washington, D.C., Mineralogical Society of America, p. 101-300.

Hammer, D. F., and Petersen, D. W., 1968, Geology of the Magma mine area, Arizona, *in* Ridge, J. D., ed., Ore Deposits of the U.S., 1933-1967, vol. 2: New York, American Institute of Mining Engineers, p. 1282-1310.

Hayba, D. O., 1997, Environment of ore deposition in the Creede mining district, San Juan Mountains, Colorado: Part V. Epithermal mineralization from fluid mixing in the OH vein: Economic Geology, v. 92, p. 29-44.

Hayba, D. O., Bethke, P. M., Heald, P., and Foley, N. K., 1985, Geologic, mineralogic, and geochemical characteristics of volcanic-hosted epithermal precious-metal deposits: Reviews in Economic Geology, v. 2, p. 129-167.

Heald, P., Foley, N. K., and Hayba, D. O., 1987, Comparative anatomy of volcanic-hosted epithermal deposits: Acid sulfate and adularia-sericite types: Economic geology, v. 82, p. 1-26.

Hedenquist, J. W., 1987, Volcanic-related hydrothermal systems in the Circum-Pacific basin and their potential for mineralisation: Mining Geology (Kozan Chishitsu), v. 37, p. 347-364.

Hedenquist, J. W., 1995, The ascent of magmatic fluid: Discharge versus mineralization, *in* Thompson, J. F. H., ed., Magmas, fluids, and ore deposits, 23, Mineralogical Association of Canada Shortcourse Series, p. 263-289.

Hedenquist, J. W., and Browne, P. R. L., 1989, The evolution of the Waiotapu geothermal system, New Zealand, based on the chemical and isotopic composition of its fluids, minerals and rocks: Geochimica et Cosmochimica Acta, v. 53, p. 2235-2257.

Hedenquist, J. W., and Lowenstern, J. B., 1994, The role of magmas in the formation of hydrothermal ore deposits: Nature, v. 370, p. 519-527.

Hedenquist, J. W., Reyes, A. G., Simmons, S. F., and Taguchi, S., 1992, The thermal and geochemical structure of geothermal and epithermal systems; a framework for interpreting fluid inclusion data: European Journal of Mineralogy, v. 4, p. 989-1015.

Hedenquist, J.W., Matsuhisa, Y., Izawa, E., White, N.C., Giggenbach, W.F., and Aoki, M., 1994a, Geology, geochemistry, and origin of high sulfidation Cu-Au mineralization in the Nansatsu district, Japan: Economic Geology, v. 89, p. 1-30.

Hedenquist, J. W., Aoki, M., and Shinohara, H., 1994b, Flux of volatiles and ore-forming metals from the magmatic-hydrothermal system of Satsuma Iwojima Volcano: Geology, v. 22, p. 585-588.

Hedenquist, J. W., Arribas, A., and Reynolds, T. J., 1998, Evolution of an intrusion-centered hydrothermal system: Far Southeast-Lepanto porphyry and epithermal Cu-Au deposits, Philippines: Economic Geology, v. 93, p. 373-404.

Hedenquist, J. W., Arribas, A., Jr., and Gonzalez-Urien, E., 2000, Exploration for epithermal gold deposits, *in* Hagemann, S. G., and Brown, P. E., eds., Gold in 2000: Reviews in Economic Geology, 13, Society of Economic Geologists, p. 245-277.

Heming, R. F., and Carmichael, I. S. E., 1973, High-temperature pumice flows from the Rabaul Caldera, Papua, New Guinea: Contributions to Mineralogy and Petrology, v. 38, p. 1-20.

Hemley, J. J., and Hunt, J. P., 1992, Hydrothermal ore-forming processes in the light of studies in rock-buffered systems: II. Some general geologic applications: Economic Geology, v. 87, p. 23-43.

Henley, R. W., and Ellis, A. J., 1983, Geothermal systems ancient and modern; a geochemical review: Earth-Science Reviews, v. 19, p. 1-50.

Henley, R. W., and McNabb, A., 1978, Magmatic vapor plumes and ground-water interaction in porphyry copper emplacement: Economic Geology, v. 73, p. 1-20.

Hezarkhani, A., and Williams-Jones, A. E., 1998, Controls of alteration and mineralization in the Sungun porphyry copper deposit, Iran: Evidence from fluid inclusions and stable isotopes: Economic Geology, v. 93, p. 651-670.

Hildreth, E. W., 1977, The magma chamber of the Bishop Tuff; gradients in temperature, pressure, and composition: unpub. Ph.D. thesis, University of California, Berkeley, 328 p.

Hildreth, W., 1981, Gradients in silicic magma chambers: Implications for lithospheric magmatism: Journal of Geophysical Research, v. 86, p. 10153-10192.

Holland, H. D., 1959, Stability relations among the oxides, sulfides, sulfates and carbonates of ore and gangue metals, Part 1: Some applications of thermochemical data to problems of ore deposits: Economic Geology, v. 54, p. 184-233.

Hunt, J. P., 1985, Applied geology at Quebrada Blanca and Collahuasi, Chile, and in the future of U.S. metal mining: Economic Geology, v. 80, p. 794-800.

Imai, A., 2001, Generation and evolution of ore fluids for porphyry Cu-Au mineralization of the Santo Thomas II (Philex) deposit, Philippines: Resource Geology, v. 51, p. 71-96.

Imai, A., Listanco, E. L., and Fujii, T., 1993, Petrologic and sulfur isotopic significance of highly oxidized and sulfur-rich magma of Mt. Pinatubo: Geology, v. 21, p. 699-702.

Inan, E. E., and Einaudi, M. T., 2002, Nukundamite ($Cu_{3.38}Fe_{0.62}S_4$)–bearing copper ore at Bingham, Utah—Result of hydrothermal upflow through quartzite: Economic Geology, v. 97, p. 499-515.

Ishihara, S., 1981, The granitoid series and mineralization, *in* Skinner, B. J., ed., Economic Geology 75th Anniversary Volume, p. 458-484.

Izawa, E., Urashima, Y., Ibaraki, K., Suzuki, R., Yokoyama, T., Kawasaki, K., Koga, A., and Taguchi, S., 1990, The Hishikari gold deposit: High-grade epithermal veins in Quaternary volcanic of southern Kyushu, Japan, *in* Hedenquist, J. W., White, N. C., and Siddeley, G., eds., Epithermal gold deposits of the Circum-Pacific, 36, Journal of Geochemical Exploration, p. 1-56.

Jannas, R. R., Bowers, T. S., Petersen, U., and Beane, R. E., 1999, High-sulfidation deposit types in the El Indio district, Chile, *in* Skinner, B. J., ed., Geology and ore deposits of the Central Andes, Society of Economic Geologists, Special Publication Number 7, p. 219-266.

Jensen, E. P., and Barton, M. D., 2000, Gold deposits related to alkaline magmatism: Reviews in Economic Geology, v. 13, p. 279-314.

John, D. A., 2001, Miocene and early pliocene epithermal gold-silver deposits in the northern Great Basin, western USA: Characteristics, distribution, and relationship to magmatism: Economic Geology, v. 96, p. 1827-1853.

John, D. A., Garside, L. J., and Wallace, A. R., 1999, Magmatic and tectonic setting of late Cenozoic epithermal gold-silver deposits in northern Nevada, with an emphasis on the Pah Rah and Virginia Ranges and the northern Nevada rift, *in* Kizis, J. A., Jr., ed., Low-sulfidation gold deposits in northern Nevada, 1999 Spring Field Trip Guidebook, Special Publication No. 29: Reno, Geological Society of Nevada, p. 64-158.

John, E. C., 1978, Mineral zones in the Utah Copper orebody: Economic Geology, v. 73, p. 1250-1259.

Johnson, J. W., Oelkers, E. H., and Helgeson, H. C., 1992, SUPCRT92; a software package for calculating the standard molal thermodynamic properties of minerals, gases, aqueous species, and reactions from 1 to 5000 bar and 0 to 1000°C: Computers & Geosciences, v. 18, p. 899-947.

Keith, J. D., Whitney, J. A., Cannan, T. M., Hook, C., and Hattori, K., 1995, The role of magmatic sulfides and mafic alkaline magmatism in the formation of giant porphyry and vein systems: Examples from the Bingham and Tintic mining districts, Utah: Giant Ore Deposits II, Kingston, Ontario, 1995, p. 350-381.

Keith, J. D., Whitney, J. A., Hattori, K., Ballantyne, G. H., Christiansen, E. H., Barr, D. L., Cannan, T. M., and Hook, C. J., 1997, The role of magmatic sulfides and mafic alkaline magmas in the Bingham and Tintic mining districts, Utah: Journal of Petrology, v. 38, p. 1679-1690.

Kiyosu, Y., 1983, Hydrogen isotopic compositions of hydrogen and methane from some volcanic areas in northeastern Japan: Earth and Planetary Science Letters, v. 62, p. 41-52.

Kooiman, G. J. A., McLeod, M.J., and Sinclair, W.D., 1986, Porphyry tungsten-molybdenum orebodies, polymetallic veins and replacement bodies, and tin-bearing greisen zones in the Fire Tower Zone, Mount Pleasant, New Brunswick: Economic Geology, v. 81, p. 1356-1373.

Kosaka, H., and Wakita, K., 1978, Some geologic features of the Mamut porphyry copper deposit, Sabah, Malaysia: Economic Geology, v. 73, p. 618-627.

Kovalenker, V. A., Safonov, Yu. G., Naumov, B. V., and Rusinov, V. L., 1997, The Kochbulak epithermal gold-telluride deposit (Uzbekistan): Geologiya Rudnykh Mestorozhdenii, v. 39, p. 127-152.

Langton, J. M., and Williams, S. A., 1982, Structural, petrological and mineralogical controls for the Dos Pobres orebody, *in* Titley, S. R., ed., Advances in geology of the porphyry copper deposits, southwestern North America: Tucson, University of Arizona Press, p. 335-352.

Le Guern, F., 1988, Ecoulements gazeux reactifs a haute temperature: measures et modelisation: unpub. These de doctorat, Université Paris 7, 314 p.

Lindgren, W., 1933, Mineral Deposits, 4th Edition: New York, McGraw-Hill, 930 p.

Lipske, J. L., and Dilles, J. H., 2000, Advanced argillic and sericitic alteration in the subvolcanic environment of the Yerington porphyry copper system, Buckskin Range, Nevada, *in* Dilles, J. H., Barton, M. D., Johnson, D. A., Proffett, J. M., and Einaudi, M. T., eds., Contrasting styles of intrusion-associated hydrothermal systems, Guidebook Series v. 32, Society of Economic Geologists, p. 91-99.

Lopez, V. M., 1939, The primary mineralization at Chuquicamata, Chile, S.A.: Economic Geology, v. 34, p. 674-711.

Losada-Calderón, A. J., and McPhail, F. C., 1996, Porphyry and high-sulfidation epithermal mineralization in the Nevados del Famatina mining district, Argentina, *in* Camus, F., Sillitoe, R. H., and Petersen, R., eds., Society of Economic Geology Special Publication, 5, p. 91-117.

MacLellan, H. E., and Taylor, R. P., 1989, Geology and geochemistry of the Burnthill Granite and related W-Sn-Mo-F mineral deposits, central New Brunswick: Canadian Journal of Earth Science, v. 26, p. 499-514.

Manske, S. L., and Paul, A. H., 2002, Geology of a major new porphyry copper center in the Superior (Pioneer) district, Arizona: Economic Geology, v. 97, p. 197-220.

Martini, M., 1993, Galeras: Bulletin of the Global Volcanism Network 18, p. 7-9.

McKinstry, H. E., 1959, Mineral assemblages in sulfide ores, the system Cu-Fe-S-O: Economic Geology, v. 54, p. 975-1001.

McKinstry, H. E., 1963, Mineral assemblages in sulfide ores, the system Cu-Fe-As-S: Economic Geology, v. 58, p. 483-505.

Melson, W. G., and Hopson, C. A., 1981, Preeruption temperatures and oxygen fugacities in the 1980 eruptive sequence: U.S. Geological Survey Professional Paper, 1250, p. 641-648.

Melson, W. G., F., A. J., Jerez, D. R., Nelen, J., and Perfit, M., 1990, Water contents, temperatures and diversity of the magmas of the catastrophic eruption of Nevado del Ruiz, Colombia, November 13, 1985: Journal of Volcanology and Geothermal Research, v. 41, p. 97-126.

Menyailov, I. A., Nikitina, L. P., and Shapar, V. N., 1984, Features in the geochemistry of magmatic gases, Great Tolbachik fissure eruption: Moscow, Nauka, p. 342-374.

Menyailov, I. A., Nikitina, L. P., Shapar, V. N., Pilipenko, V. P., Sato, M., Matsuo, S., and King, C.-Y., 1986, Temperature increase and chemical change of fumarolic gases at Momotombo Volcano, Nicaragua, in 1982-1985; are these indicators of a possible eruption?: Journal of Geophysical Research, v. 91, p. 12,199-12,214.

Merwin, H. E., and Lombard, R. H., 1937, the system Cu-Fe-S: Economic Geology, v. 32, p. 203-284.

Meyer, C., and Hemley, J. J., 1967, Wall-rock alteration, in Barnes, H. L., ed., Geochemistry of hydrothermal ore deposits: New York, Holt, Rinehart, and Winston, p. 166-235.

Meyer, C., Shea, E. P., and Goddard, C. C., Jr., 1968, Ore deposits at Butte, Montana, in Ridge, J. D., ed., Ore Deposits of the U.S., 1933-1967, vol. 2: New York, American Institute of Mining Engineers, p. 1373-1416.

Mizutani, Y., and Sugiura, T., 1982, Variations in chemical and isotopic compositions of fumarolic gases from Showashinzan Volcano, Hokkaido, Japan: Geochemical Journal, v. 16, p. 63-71.

Mizutani, Y., Hayashi, S., and Sugiura, T., 1986, Chemical and isotopic compositions of fumarolic gases from Kuju-Iwoyama, Kyushi, Japan: Geochemical Journal, v. 20, p. 273-285.

Myers, J., and Eugster, H. P., 1983, The system Fe-Si-O: Oxygen buffer calibrations to 1,500 K: Contributions to Mineralogy and Petrology, v. 82, p. 76-90.

Muntean, J. L., and Einaudi, M. T., 2001, Porphyry-epithermal transition: Maricunga Belt, northern Chile: Economic Geology, v. 96, p. 743-772.

Neumann, E., 1976, Compositional relations among pyroxenes, amphiholes and other mafic phases in the Oslo Region plutonic rocks: Lithos, v. 9, p. 85-109.

Nordlie, B. E., Thieben, S. E., Burggraf, D. R., Pepin, R. O., and O'Connell, R. J., 1983, Equilibrium composition of the Mt. St. Helens magmatic volatile phase from the pyrrhotite-magnetite assemblage, in Conference on planetary volatiles: Houston, Lunar and Planetary Institute, p. 122-130.

Ohba, T., Hirabayashi, J-I., and Yoshida, M., 1994, Equilibrium temperature and redox state of volcanic gas at Unzen volcano, Japan: Journal of Volcanology and Geothermal Research, v. 60, p. 263-272.

Ohmoto, H., and Rye, R. O., 1979, Isotopes of sulfur and carbon, in Barnes, H. L., ed., Geochemistry of hydrothermal ore deposits, Second Edition: New York, Holt, John Wiley & Sons, p. 517-611.

Ohmoto, H., and Goldhaber, M.B., 1997, Sulfur and carbon isotopes , in Barnes, H. L., ed., Geochemistry of hydrothermal ore deposits, Third Edition: New York, John Wiley & Sons, p. 737-796.

Ossandón, C. G., Fréraut, C. R., Gustafson, L. B., Lindsay, D. D., and Zentilli, M., 2001, Geology of the Chuquicamata mine: A progress report: Economic Geology, v. 96, p. 249-270.

Petersen, Ulrich, 1965, Regional geology and major ore deposits of central Peru: Economic Geology, v. 60. p. 407-476.

Pollard, P. J., and Taylor, R. G., 2002, Paragenesis of the Grasberg Cu-Au deposit, Irian Jaya, Indonesia: results from logging section 13: Mineralium Deposita, v. 37, p. 117-136.

Poorter, R. P. E., Varekamp, J. C., Poreda, R. J., van Bergen, M. J., and Kreulen, R., 1991, Chemical and isotopic compositions of volcanic gases from the East Sunda and Banda arcs, Indonesia: Geochimica et Cosmochimica Acta, v. 55, p. 3795-3807.

Preece, R. K., III, and Beane, R. E., 1982, Contrasting evolutions of hydrothermal alteration in quartz monzonite and quartz diorite wall rocks at the Sierrita porphyry copper deposit, Arizona: Economic Geology, v. 77, p. 1621-1641.

Proffett, J. M., Jr., 1979, Ore deposits of the western United States: A summary: Nevada Bureau of Mines and Geology, Report 33, p. 13-32.

Ransome, F. L., 1907, The association of alunite with gold in the Goldfield district, Nevada: Economic Geology, v. 2, p. 667-692.

Ransome, F. L., 1909, The geology and ore deposits of Goldfield, Nevada, U.S. Geological Survey, Professional Paper 66, 258 p.

Redmond, P. B., Landtwing, M. R., and Einaudi, M. T., 2001, Cycles of porphyry dike emplacement, veining, alteration, and mineralization in the Bingham porphyry Cu-Au-Mo deposit, Utah, *in* Piestrzinsky, A., et al., ed., Mineral Deposits at the beginning of the 21st Century, Proceeding Joint 6th Biennial SGA-SEG Meeting, Krakow, Poland, 26-29 Aug 01, A.A. Balkema Publishers, p. 473-476.

Reed, M. H., 1997, Hydrothermal alteration and its relationship to ore fluid composition, *in* Barnes, H. L., ed., Geochemistry of hydrothermal ore deposits: New York, John Wiley & Sons, p. 303-365.

Reyes, A.G., Giggenbach, W.F., Saleras, J.R.M., Salonga, N.D., and Vergara, M.C., 1993, Petrology and geochemistry of Alto Peak, a vapor-cored hydrothermal system, Leyte province, Philippines: Geothermics, v. 22, p. 479-519.

Reynolds, T.J., and Beane, R.E., 1985, Evolution of hydrothermal fluid characteristics at the Santa Rita, New Mexico, porphyry copper deposit: Economic Geology, v. 80, p. 1328-1347.

Richards, J. P., 1995, Alkalic-type epithermal gold deposits, a review: Mineralogical Association of Canada Short Course Series, v. 23, p. 367-400.

Rowins, S. M., 2000, Reduced porphyry copper-gold deposits: A new variation on an old theme: Geology, v. 28, p. 491-494.

Rutherford, N. F., and Heming, R. F., 1978, The volatile component of Quaternary ignimbrite magmas from the North Island, New Zealand: Contributions to Mineralogy and Petrology, v. 65, p. 401-411.

Sales, R. H., and Meyer, C., 1949, Results from preliminary studies of vein formation at Butte, Montana: Economic Geology, v. 44, p. 465-484.

Samson, I. M., 1990, Fluid evolution and mineralization in a subvolcanic granite stock: the Mount Pleasant W-Mo-Sn deposits, New Brunswick, Canada: Economic Geology, v. 85, p. 145-163.

Saunders, J. A., 1994, Silica and gold textures in bonanza ores of the Sleeper deposit, Humboldt County, Nevada: Evidence for colloids and implications for epithermal ore-forming processes: Economic Geology, v. 89, p. 628-638.

Schmidt, H., 1950, The fumarolic hot spring and epithermal mineral deposit environment: Quarterly of the Colorado School of Mines, v. 45, p. 209-229.

Scott, S. D., and Barnes, H. L., 1971, Sphalerite geothermometry and geobarometry: Economic Geology, v. 66, p. 653-669.

Seedorff, Eric, 1988, Cyclic development of hydrothermal mineral assemblages related to multiple intrusions at the Henderson porphyry molybdenum deposit, Colorado, *in* Taylor, R. P., and Strong, D. F., eds., Recent advances in the geology of granite-related mineral deposits, 39: Halifax, Canadian Institute of Mining and Metallurgy - Special Volume, p. 367-393.

Sherlock, R. L., Tosdal, R. M., Lehrman, N. J., Graney, J. R., Losh, S., Jowett, E. C., and Kesler, S. E., 1995, Origin of the McLaughlin mine sheeted vein complex: Metal zoning, fluid inclusion and isotopic evidence: Economic Geology, v. 90, p. 2156-2181.

Shinohara, H., 1994, Exsolution of immiscible vapor and liquid phases from a crystallizing silicate melt: Implications for chlorine and metal transport: Geochimica et Cosmochimica Acta, v. 58, p. 5215-5221.

Shinohara, H., Giggenbach, W. F., Kazahaya, K., Hedenquist, J. W., and Kusakabe, M., 1993, Geochemistry of volcanic gases and hot springs of Satsuma-Iwojima, Japan: following Matsuo: Geochemical Journal, v. 27, p. 271-285.

Sillitoe, R. H., 1973, The tops and bottoms of porphyry copper deposits: Economic Geology, v. 68, p. 799-815.

Sillitoe, R. H., 1983, Enargite-bearing massive sulfide deposits high in porphyry copper systems: Economic Geology, v. 78, p. 348-352.

Sillitoe, R. H., 1995, Exploration of porphyry copper lithocaps, *in* Mauk, J.L., and St. George, J.D., eds., PACRIM Congress 1995: Australasian Institute of Mining and Metallurgy, Publication Series No. 9/95, p. 527-532.

Sillitoe, R. H., 1999, Exploration and discovery of base- and precious-metal deposits in the circum-Pacific region during the last 25 years, Resource Geology Special Issue 19, 119 p.

Sillitoe, R.H., 2002, Rifting, bimodal volcanism, and bonanza gold veins: Society of Economic Geologists Newsletter, no. 48, p. 24-26.

Sillitoe, R. H., and Hedenquist, J. W., 2002, Linkages between volcanotectonic settings, ore-fluid compositions, and epithermal precious-metal deposits: this volume.

Spencer, K. J., and Lindsley, D. H., 1981, A solution model for coexisting iron-titanium oxides: American Mineralogist, v. 66, p. 1189-1201.

Stein, H. J., 1988, Genetic traits of Climax-type granites and molybdenum mineralization, Colorado Mineral Belt, *in* Taylor, R. P., and Strong, D. F., eds., Recent advances in the geology of granite-related mineral deposits, 39: Halifax, Canadian Institute of Mining and Metallurgy - Special Volume, p. 394-401.

Stoffregen, R. E., 1987, Genesis of acid-sulfate alteration and Au-Cu-Ag mineralization at Summitville, Colorado: Economic Geology, v. 82, p. 1575-1591.

Symonds, R. B., Rose, W. I., Gerlach, T. M., Briggs, P. H., and Harmon, R. S., 1990, Evaluation of gases, condensates, and SO_2 emissions from Augustine Volcano, Alaska; the degassing of a Cl-rich volcanic system: Bulletin of Volcanology, v. 52, p. 355-374.

Taran, Y., Fischer, T. P., Pokrovsky, B., Sano, Y., Armienta, M. A., and Macias, J. L., 1998, Geochemistry of the volcano-hydrothermal system of El Chichón Volcano, Chiapas, Mexico: Bulletin of Volcanology, v. 59, p. 436-449.

Taran, Y. A., Hedenquist, J. W., Korzhinsky, M. A., Tkachenko, S. I., and Shmulovich, K. I., 1995, Geochemistry of magmatic gases from Kudryavy Volcano, Iturup, Kuril Islands: Geochimica et Cosmochimica Acta, v. 59, p. 1749-1761.

Taran, Y. A., Pilipenko, V. P., Rozhkov, A. M., and Vakin, E. A., 1992, A geochemical model for fumaroles of the Mutnovsky Volcano, Kamchatka, USSR: Journal of Volcanology and Geothermal Research, v. 49, p. 269-283.

Taran, Y. A., Rozhkov, A. M., Serafimova, E. K., and Esikov, A. D., 1991, Chemical and isotopic composition of magmatic gases from the 1988 eruption of Klyuchevskoy Volcano, Kamchatka: Journal of Volcanology and Geothermal Research, v. 46, p. 255-263.

Taylor, R. P., Lux, D. R., MacLellan, H. E., and Hubacher, F., 1987, Age and genesis of granite-related W-Sn-Mo mineral deposits, Burnthill, New Brunswick, Canada: Economic Geology, v. 82, p. 2187-2198.

Thompson, J. F. H., and Newberry, R. J., 2000, Gold deposits related to reduced granitic intrusions, *in* Hagemann, S. G., and Brown, P. E., eds., Gold in 2000, Reviews in Economic Geology 13, Society of Economic Geologists, p. 377-400.

Toulmin, P., III, and Barton, P. B., Jr., 1964, A thermodynamic study of pyrite and pyrrhotite: Geochimica et Cosmochimica Acta, v. 28, p. 641-671.

Ueda, A., and Itaya, T., 1981, Microphenocrystic pyrrhotite from dacite rocks of Satsuma-Iwojima, Southwest Kyushu, Japan and the solubility of sulfur in dacite magma: Contributions to Mineralogy and Petrology, v. 78, p. 21-26.

Ulrich, T., and Heinrich, C. A., 2001, The evolution of a porphyry Cu-Au deposit, based on LA-ICP-MS analysis of fluid inclusions: Bajo de la Alumbrera, Argentina: Economic Geology, v. 96, p. 1743-1774.

Watanabe, Y., and Hedenquist, J. W., 2001, Mineralogic and stable isotope zonation at the surface over the El Salvador porphyry copper deposit, Chile: Economic Geology, v. 96, p. 1775-1797.

West, R. J., and Aiken, D. M., 1982, Geology of the Sierrita-Esperanza deposit, Pima mining district, Pima county, Arizona, *in* Titley, S. R., ed., Advances in geology of the porphyry copper deposits, southwestern North America: Tucson, University of Arizona Press, p. 433-465.

White, D. E., 1981, Active geothermal systems and hydrothermal ore deposits: Economic Geology, 75th Anniversary Volume, p. 392-423.

White, D. E., Muffler, L.J.P., and Truesdell, A.H., 1971, Vapor-dominated systems compared with hot-water systems: Economic Geology, v. 66, p. 75-97.

White, N. C., and Hedenquist, J. W., 1990, Epithermal environments and styles of mineralization: variations and their causes, and guidelines for exploration: Journal of Geochemical Exploration, v. 36, p. 445-474.

Whitney, J. A., 1984, Fugacities of sulfurous gases in pyrrhotite-bearing silicic magmas: American Mineralogist, v. 69, p. 69-78.

Whitney, J. A., and Stormer, J. C., 1983, Igneous sulfides in the Fish Canyon Tuff and the role of sulfur in calc-alkaline magmas: Geology, v. 11, p. 99-102.

Wolff, J. A., and Storey, M., 1983, The volatile component of some pumice-forming alkaline magmas from the Azores and Canary Islands: Contributions to Mineralogy and Petrology, v. 82, p. 66-74.

Wones, D. R., 1981, Mafic silicates as indicators of intensive variables in granitic magmas: Mining Geology, v. 31, p. 191-212.

Xirouchakis, D., Lindsley, D. H., and Frost, B. R., 2001, Assemblages with titanite ($CaTiOSiO_4$), Ca-Mg-Fe olivine and pyroxenes, Fe-Mg-Ti oxides and quartz; Part II, Application: American Mineralogist, v. 86, p. 254-264.
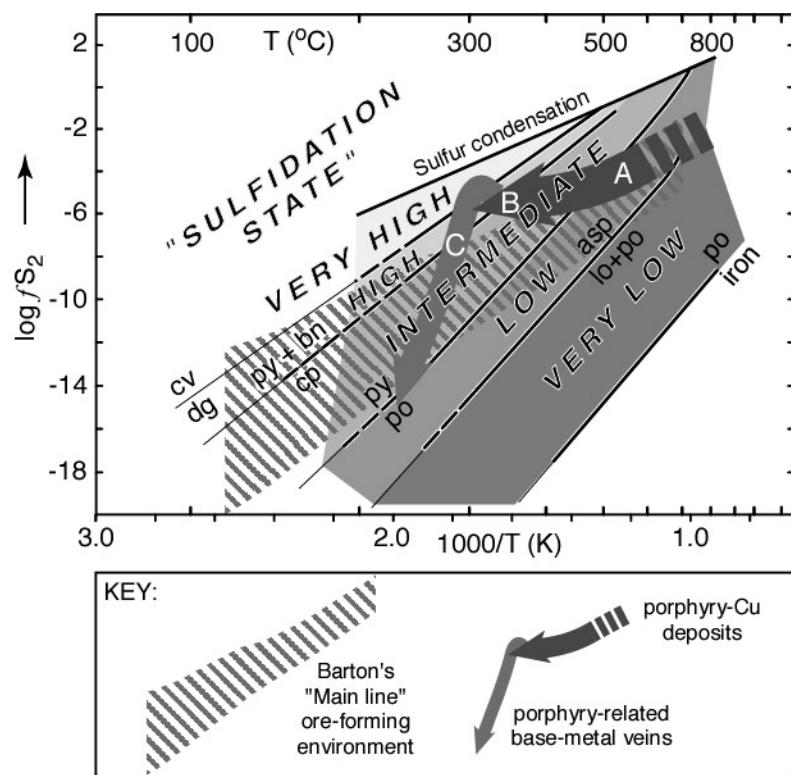
Figures

Fig. 1. Log fS_2 – 1000/T diagram defining the relative sulfidation state of hydrothermal fluids, the Main Line ore-forming environment from Barton (1970), and the evolutionary path of fluids in porphyry copper and porphyry-related vein deposits (see text for discussion of A, B, and C). lo = loellingite; other abbreviations in Table 4. Sulfidation reactions from Barton and Skinner (1979).
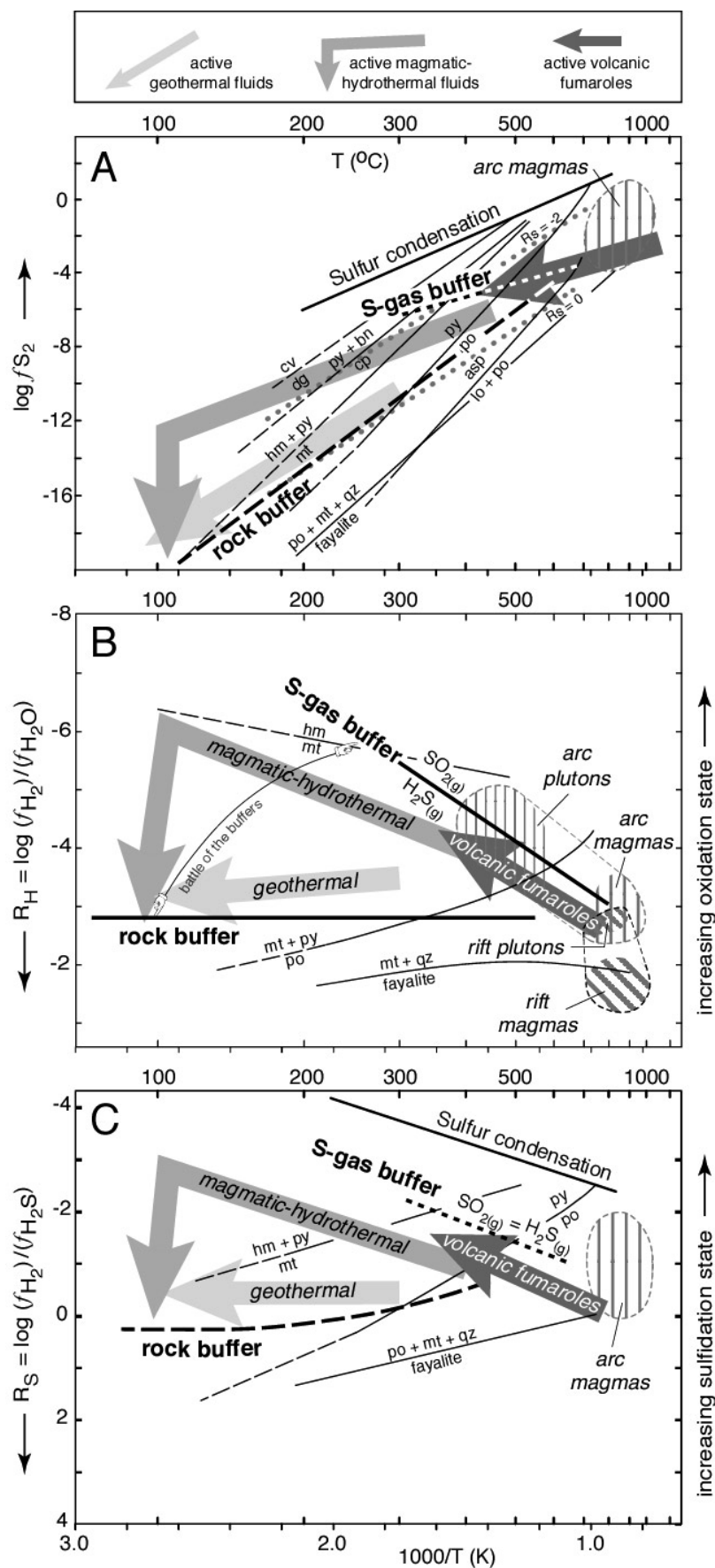
Fig. 2. Generalized log fS_2 – 1000/T (A), R_H - 1000/T (B), and R_S – 1000/T (C) diagrams illustrating the interrelation between these diagrams and the generalized sulfidation and redox state of arc magmas and compositional trends of hydrothermal fluids from active systems. Positions of sulfur-gas buffer and rock buffer (see text) in A and C are speculative. Based on Figures 3, 4, and 5.
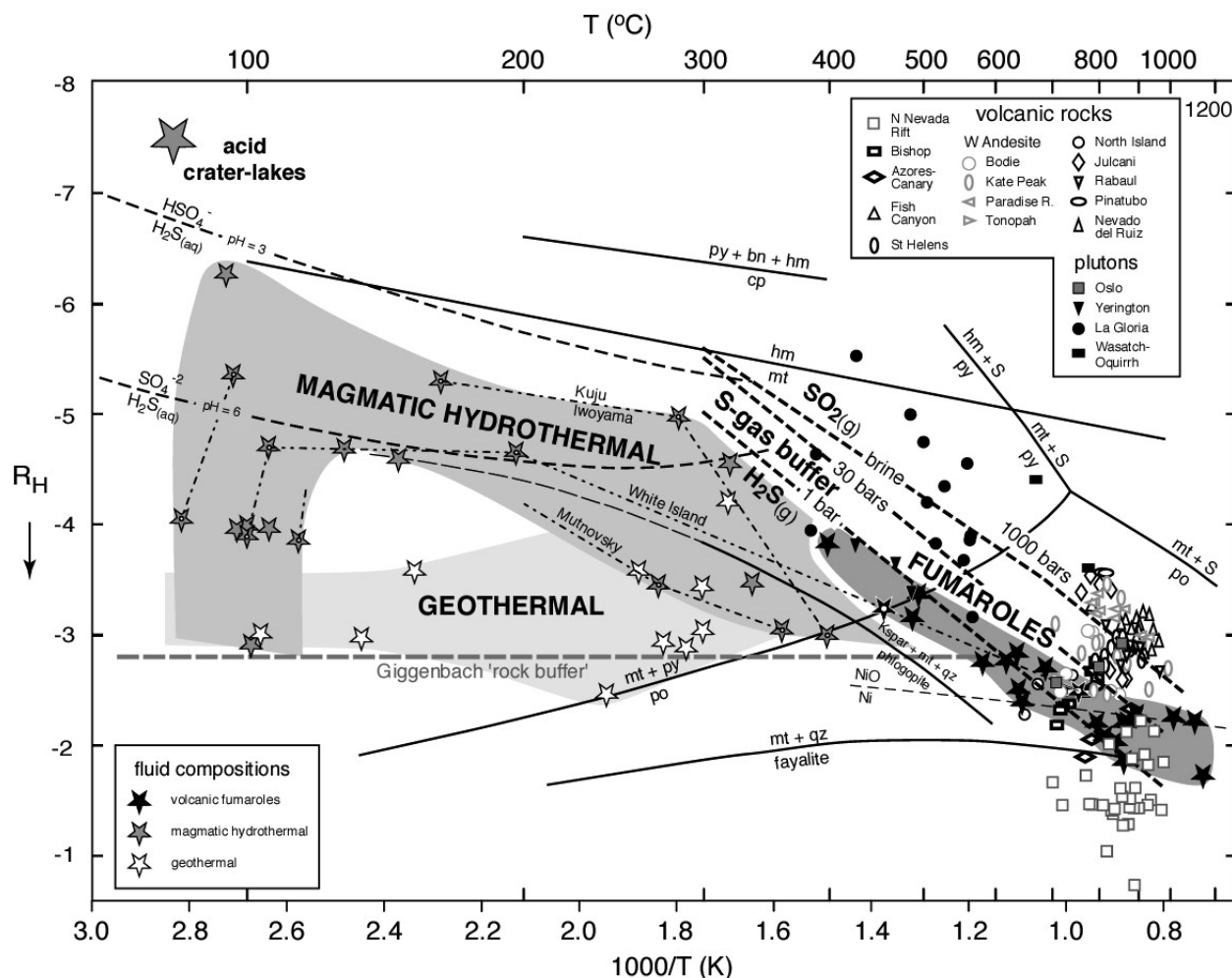
Fig. 3. R_H - 1000/T diagram showing redox states of magmas (Table 2) and fluids from active hydrothermal systems at 1 bar (Table 3), plotted over a grid of mineral reactions at 500 bars. Fluid compositions are deemed representative of their type, based on compilations or the original source, as referenced in Table 3. Dash-dot lines join fluid compositions from the same locality. Large star indicates composition of volcanic crater lakes (Giggenbach, 1992). The "rock buffer" and sulfur-gas buffer (isomolar $SO_{2(g)} = H_2S_{(g)}$) are from (Giggenbach, 1987). The predominance boundary $H_2S = HSO_4^-$ at pH = 3 is relevant to magmatic-hydrothermal fluids; the boundary $H_2S = SO_4^=$ at pH = 6 is relevant to geothermal fluids. Mineral abbreviations: Kspar = K feldspar; all others as in Table 4. See Appendix for further details on data sources and method of calculation.
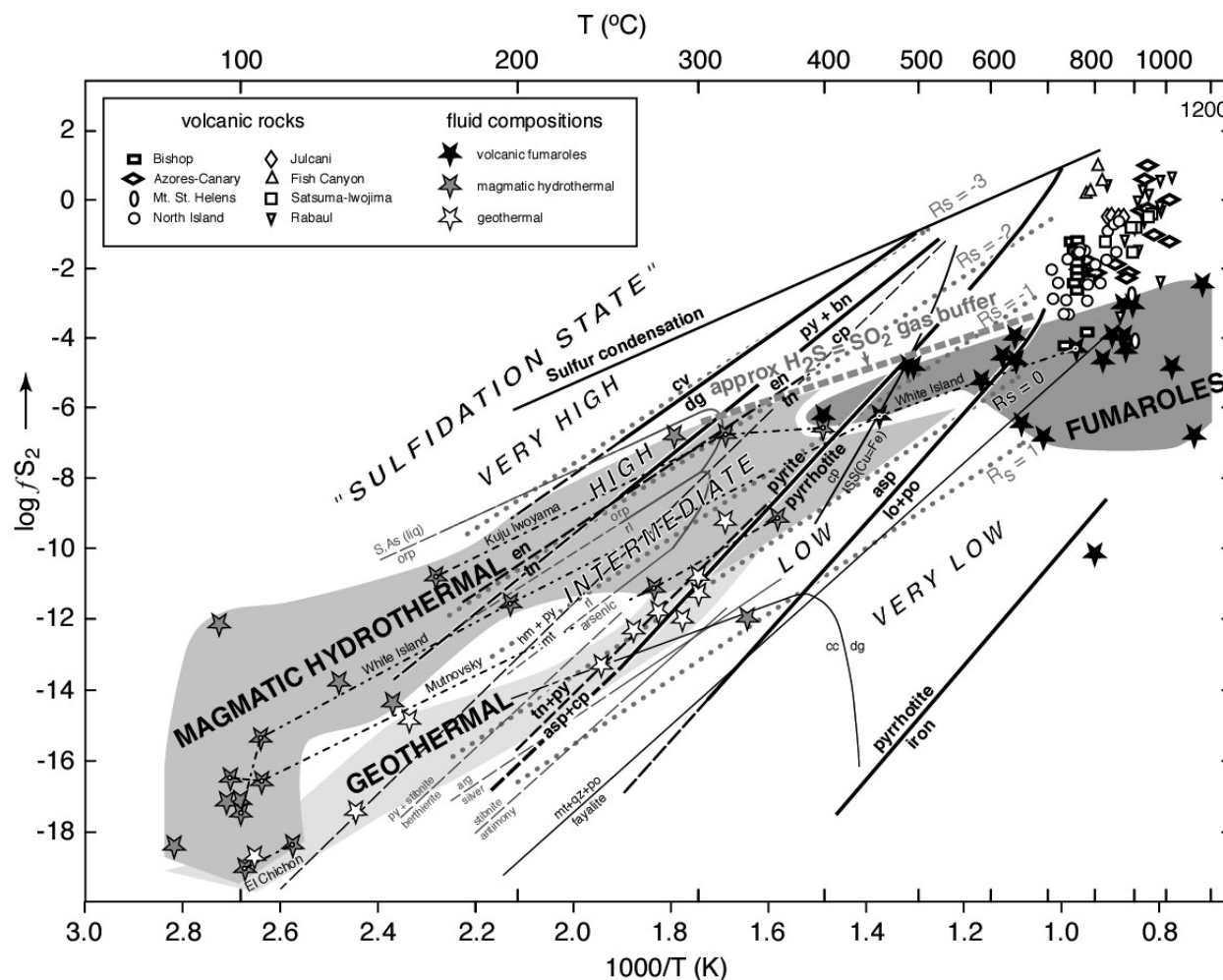
Fig. 4. Log fS_2 – 1000/T diagram, contoured for R_S, showing sulfidation state of magmas (Table 2) and fluids from active hydrothermal systems (Table 3) plotted over a grid of mineral sulfidation reactions at 1 bar. Dash-dot lines join fluid compositions from the same locality. Sulfidation states of magmas are based on pyrrhotite compositions in volcanic rocks using equations in Toulmin and Barton (1964) and Scott and Barnes (1971) combined with temperature estimates as in Figure 3. Sulfidation reactions used to define sulfidation states and those representing limits to assemblages commonly cited in the text are in bold; all sulfidation reactions are from Barton and Skinner (1979) and Myers and Eugster (1983) at 1 bar pressure with the exception of reaction tn = en which is based on natural occurrence (see text). See Table 4 for mineral abbreviations, and Appendix for details of calculations.
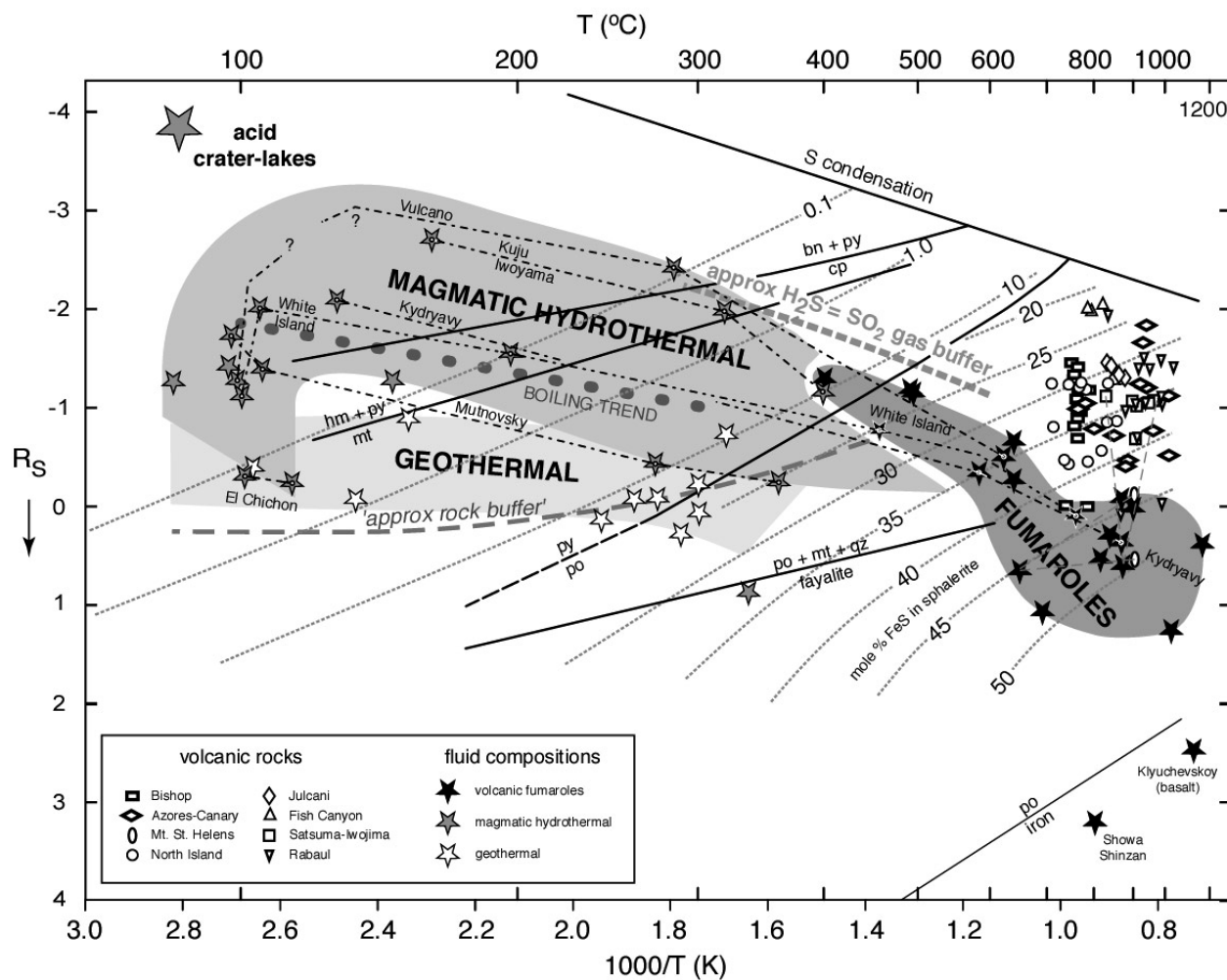
Fig. 5. R_S – 1000/T diagram showing sulfidation state of magmas (Table 2) and fluids from active hydrothermal systems (Table 3) plotted over a grid of mineral sulfidation reactions at 1 bar. R_S – 1000/T values for volcanic rocks as in Fig. 4 (sources in Table 2). Dash-dot lines join fluid compositions from the same locality. The trend expected for a liquid boiling from 300 to 150°C is based on data in Giggenbach (1980; see Appendix). $SO_2 = H_2S$ gas buffer and Giggenbach's "rock buffer" cannot be calculated in terms of R_S and are approximated from their positions in Figure 3. Mineral reactions are from Barton and Skinner (1979) and Myers and Eugster (1983). Contours of mole percent FeS in sphalerite coexisting pyrrhotite or pyrite are from Scott and Barnes (1971) and Czamanske (1974). See Table 4 for mineral abbreviations and Appendix for log fS_2 to R_S conversion.
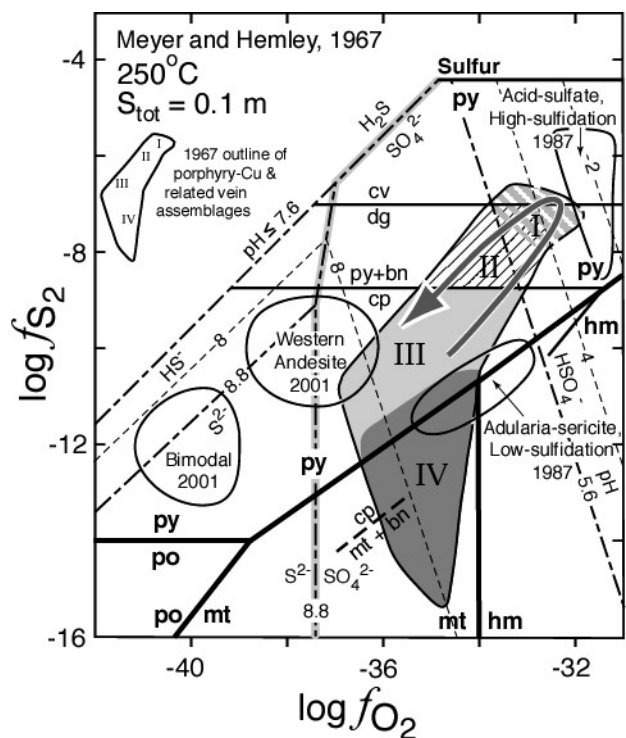
Fig. 6. Log fS_2 – Log fO_2 diagram at 250°C modified from Meyer and Hemley (1967) illustrating the looping path through time and space in porphyry and porphyry-related vein deposits. Lines of constant pH are dashed (bold where signifying predominance boundaries between aqueous sulfur species). Fields defined and labeled with roman numerals by Meyer and Hemley are: I. Covellite, digenite, chalcocite, and pyrite with advanced argillic or sericitic alteration; II. Chalcocite, bornite, pyrite, or chalcopyrite, bornite, pyrite with zoned sericitic and intermediate argillic alteration; III. Chalcopyrite + pyrite with zoned sericitic (relict K feldspar) and intermediate argillic; and IV. Chalcopyrite + magnetite, or bornite + magnetite with potassic alteration. Also shown are fields for the epithermal deposits from Heald et al. (1987) and John (2001). Mineral abbreviations as in Table 4.
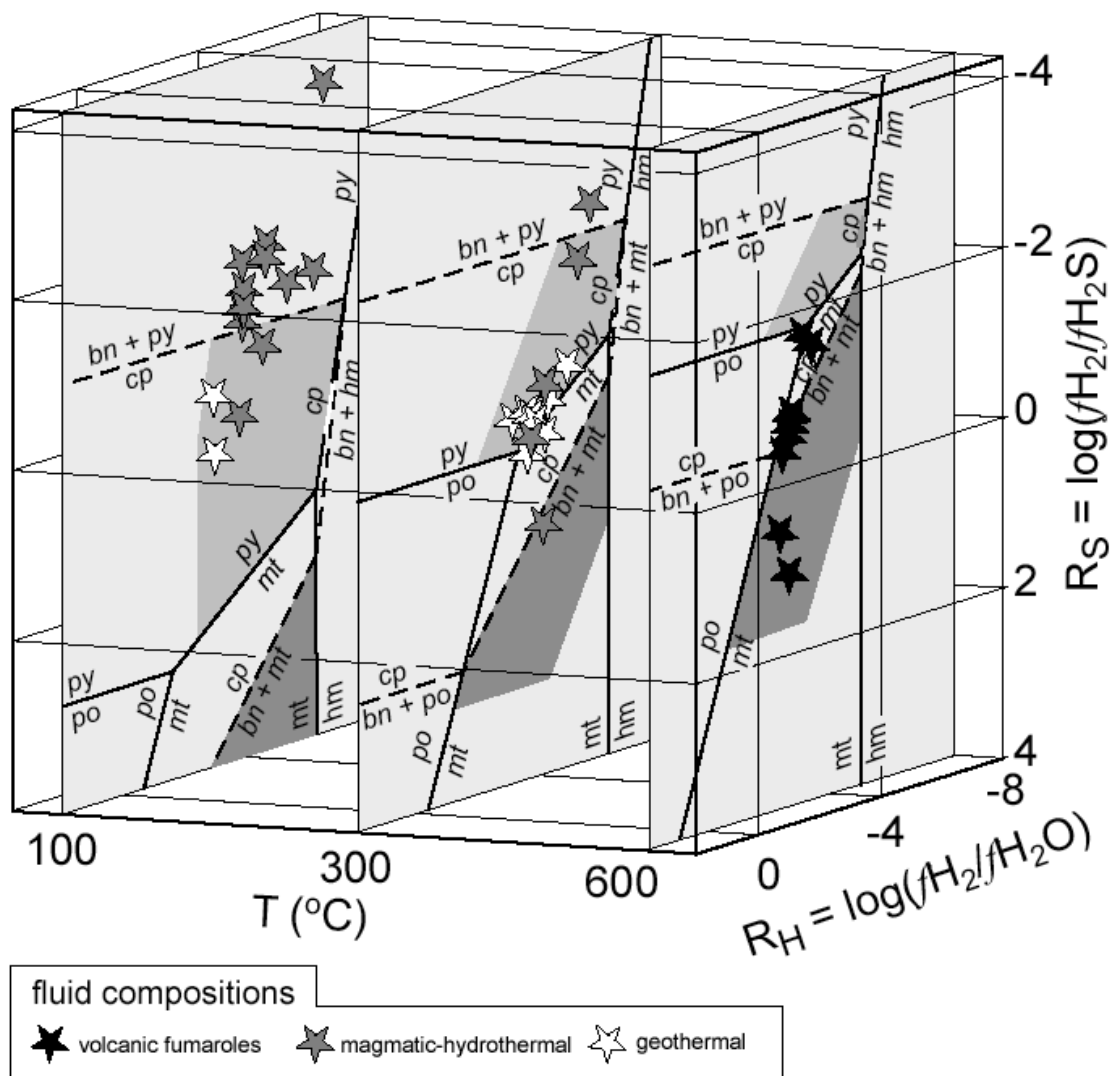
Fig. 7. R_S – R_H -T diagram constructed at 600, 300 and 100°C illustrating compositional relations between fluids from active systems and phase equilibria in the system Cu-Fe-S-O. Stability fields of bornite + magnetite and chalcopyrite + pyrite are highlighted by dark and medium shading, respectively. Fluid compositions from Table 3 are plotted on isothermal sections by projection along the average slope of tie-lines shown on Figures 3 and 5. Thermal windows used are: 900 to 440°C projected onto the 600°C section; 360 to 240°C onto the 300°C section; and 155 to 82°C onto the 100°C section. At 600°C the bulk fluid plots in the magnetite + bornite ± chalcopyrite field, at 300°C it straddles the chalcopyrite + magnetite and chalcopyrite + pyrite fields, and at 100°C it straddles the pyrite + chalcopyrite and pyrite + bornite ± digenite fields, a pattern that is consistent with assemblages documented in porphyry, porphyry-related vein deposits, and some epithermal deposits (Table 4). Phase relations among stoichiometric Cu-Fe-S-O minerals based on data in Barton and Skinner (1979) and Myers and Eugster (1983) recalculated to R_S and R_H as discussed in Appendix.
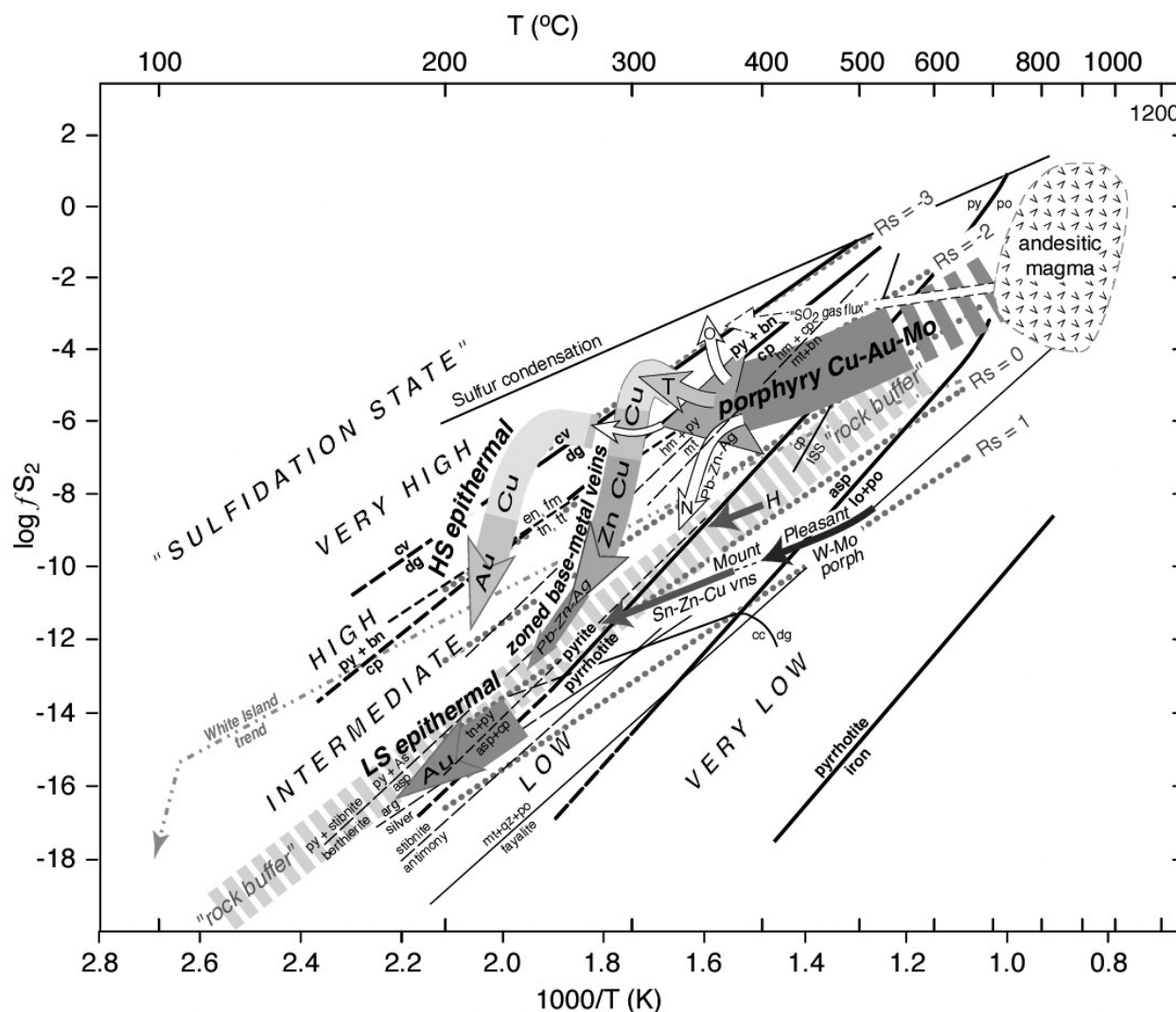
Fig. 8. Log fS$_2$ – 1000/T diagram, contoured for R$_S$, illustrating fluid environments in porphyry copper, porphyry-copper related base-metal veins, and epithermal Au-Ag deposits in terms of a series of possible cooling paths that are influenced by processes discussed in text. Fluid environments are based on sulfide assemblages summarized in Table 4, temperatures discussed in text, and sulfidation reactions from Barton and Skinner (1979). Arrow labeled "porphyry Cu-Au-Mo" refers to early- and intermediate-age assemblages deposited at approximately 500 to 350°C and low to intermediate sulfidation states. Arrows labeled "N" and "O" represent deviations from the main-line environment. Transition to late assemblages at high sulfidation states and to porphyry-related "zoned base-metal veins" at or below 350°C is indicated by gray arrow labeled "T". Sulfide assemblages in the latter deposits describe a return from very high sulfidation to the intermediate sulfidation states of the "rock buffer". Similarly, HS epithermal deposits consist of an early Cu-rich, high sulfidation state assemblage followed by a Au-rich stage at intermediate sulfidation states. IS epithermal deposits (not shown) form at about 250 °C and mostly at intermediate sulfidation states. LS epithermal gold veins are shown near 200 °C and at low to intermediate sulfidation states near the rock buffer. Other porphyry-type deposits that form at low and even very low sulfidation states (dark, thin arrows labeled "Mount Pleasant" W-Mo and related Sn-Zn-Cu veins, and parts of Henderson Mo (labeled "H"; see text) are shown for contrast to porphyry Cu and related vein deposits.

Appendix

Calculation of Mineral and Gas Equilibria

Rock, mineral, and gas buffer curves

All redox data for volcanic and plutonic rocks (Table 2) are based on assemblages involving pyroxenes, iron-titanium oxides and titanite. Most have been recalculated in terms of T and log fO_2 for internal consistency using QUILF (Andersen et al., 1991; Andersen et al., 1993).

Giggenbach's (1997) "rock buffer" (Fig. 3) is based on the relation

$$4 \; FeO_{1.5} = 4 \; FeO + O_2, \tag{A1}$$

with $a_{(FeO)} / a_{(FeO1.5)}) = 1$. This buffer approximates the average R_H value of subduction-related calc-alkaline magmas, and at 400 to 600°C it is close to both Ni + NiO and K feldspar + magnetite + quartz + phlogopite (mole fraction annite = 0.2).

Mineral equilibria plotted in Figures 3 and 5 and listed below (Table A) were calculated at 500 bars pressure using SUPCRT92 (Johnson et al., 1992) with the exception of hematite-bearing reactions (Figs. 3 & 5) which were adjusted with equation 14 of Myers and Eugster (1983) in order to be consistent with prior R_H and R_S diagrams published by Giggenbach.

In the system Fe-S-O (Fig. 3), only the phase relations involving magnetite (or hematite) are shown for reference to magnetite-bearing igneous rocks; the stability field of $FeSO_4$ is ignored. Location of invariant point magnetite + hematite + pyrite + pyrrhotite + $s_{(l)}$ is based on the calculated intersection of the reactions pyrite = pyrrhotite + $s_{(l)}$ and pyrite = magnetite + $s_{(l)}$.

The $SO_{2(g)} = H_2S_{(g)}$ isomolar curve ("sulfur-gas buffer"),

$$2/3 \; H_2S_{(gas)} + O_2 = 2/3 \; SO_{2(gas)} + 2/3 \; H_2O, \tag{A2}$$
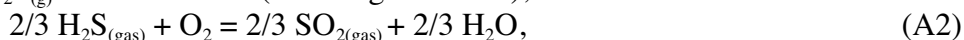
plotted on log (fH_2 / fH_2O) – 1000/T (Fig. 3),was calculated using standard equilibrium constants of formation at different total pressures (D. R. Stull, 1969, in Giggenbach, 1987).

The equilibrium boiling trend for residual liquid (pure water) illustrated in Figure 5 was calculated from 300ºC to 100ºC using vapor-liquid gas distribution coefficients for H_2 and H_2S from Table 2 of Giggenbach (1980). The boiling trend reflects the higher solubility of H_2 relative to H_2S in the vapor phase.

Recalculation of total discharge (Table 3)

We calculated R_H and R_S values for the wells listed in Table 3, which were reported for total discharge (all at temperatures <300ºC), to allow comparison with vapors discharged from fumaroles. Calculations used temperature-dependent vapor-liquid gas distribution coefficients, B_i = $x_{v,i} / x_{l,i}$ for H_2 and H_2S from Table 2 of Giggenbach (1980).

Justification of $R_H \approx log \, (XH_2 / XH_2O)$ and $R_S \approx log \, (XH_2 / XH_2S)$ for modern fluids

We follow Giggenbach (1987, p. 146-147) in making the assumption that for gases in which H_2O is the major component, the uncorrected analytical mole ratio (e.g., XH_2 / XH_2S) is approximately equivalent to the fugacity ratio (e.g., fH_2 / fH_2S). That is, the ratio of the activity coefficients do not deviate much from unity. This assumption introduces unknown errors in comparing analytical R_H and R_S values for fluids with computed R_H and R_S values for mineral reactions (Figs. 3, 4 and 5).

R_H and log fO_2

 Log $fO2$ values calculated for rocks, mineral reaction curves, the sulfur-gas buffer, and the predominance boundaries for aqueous sulfur species (Table A) were converted to R_H, where R_H = log (fH_2 / fH_2O), using equation 15.6 of Giggenbach (1997):

$$\log fO_2 = 5.3 - 25{,}552/T - 2\ R_H, \tag{A3}$$

for T in Kelvins.

R_S and log fS_2

 Log fS_2 values calculated for sulfide mineral reactions were converted to R_S, where R_S = log (fH_2 / fH_2S), in Figure 5, and R_S values for fluids given in Table 3 were converted to log fS_2 values in Figure 4, on the basis of the free energy change for the reaction

$$2\ H_2S_{(g)} = 2\ H_{2(g)} + S_{2(g)} \tag{A4}$$

at 1 bar (Barton and Skinner, 1979), yielding the expression

$$\log fS_2 = 4.9 - 9{,}251/T - 2\ R_S, \tag{A5}$$

for T in Kelvins.

Approximate sulfur-gas buffer on log fS_2 – 1/T and R_S – 1/T plot

 The relation

$$2/3\ H_2S_{(g)} + 4/3\ H_2O + S_2 = 2/3\ SO_{2(g)} + 2\ H_2S_{(aq)} \tag{A6}$$
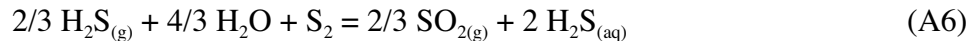
can be used to plot the sulfur-gas buffer on a log fS_2 – 1000/T diagram at constant $aH_2S_{(aq)}$ and constant pressure (Inan and Einaudi, 2002). Reaction A6 has a moderately negative slope on a log fS_2 – 1000/T diagram, indicating that if a hydrothermal fluid were to cool along the sulfur-gas buffer at constant pressure and constant $aH_2S_{(aq)}$, then the sulfidation state would increase at a significantly higher rate than is documented by active magmatic-hydrothermal systems or deduced from sulfide assemblages in ore deposits formed at T > 350ºC. In order to achieve a log fS_2 – 1/T trajectory such as shown on Figures 1, 2A, 4, and 8 above 350ºC and retain $SO_{2(g)}/H_2S_{(g)}$ = 1, hydrothermal fluids must depressurize, and/or loose sulfur. Such changes, appropriate for the high-temperature porphyry environment, could lead to the relatively flat trajectories shown on Figures 4 and 5 as "approximate $SO_{2(g)} = H_2S_{(g)}$ gas buffer".

Tables

Table 1. History of concepts involving the aqueous S-H-O system and sulfidation state as applied to fluids and mineral assemblages in porphyry Cu and epithermal Au-Ag deposits

Concept or Process	Definition or Conclusion	Sources	Comments
1906-1909 Hypogene alunite in epithermal ores	"Direct volcanic hypothesis", ore solutions emanated from magma, acid and then neutralized by reaction with rock. Later changed to "solfatarism and oxidation model", alunite formed by oxidation of magmatic aqueous sulfur in the near-surface.	Ransome, 1907, 1909	Recognized presence of chemically distinct epithermal environments following study of Goldfield deposit, Nevada; interpreted close association of alunite with ore minerals as result of acidic hypogene fluid related to fumaroles from degassing magma.
1933 Classification of epithermal deposits	Deposits classed on the basis of ore mineralogy as either gold-, silver-, or base-metal rich.	Lindgren, 1933	Concluded that epithermal deposits formed from near neutral-pH waters similar to those discharged from hot springs; qualifyingly accepted Ransome's alunite-quartz type.
1933-1950	Magmatic-hydrothermal fluids start off acid and become alkaline as they react with their wall rock.	Bowen, 1933; Fenner, 1933	Acidic origins of magmatic-hydrothermal fluids, based on studies of Yellowstone hot springs, contrary to Graton (below).
Alkaline or acid magmatic volatiles?	Magmatic-hydrothermal fluids start off alkaline and become acid through boiling and hydrolysis of H_2S.	Graton and Bowditch, 1936	Alkaline origins of magmatic-hydrothermal fluids, based on studies of base-metal ores at Cerro de Pasco, Peru, contrary to Bowen and Fenner (above).
Hot springs-epithermal analogy	From explosive volcanic phenomena and fumaroles to geysers and hot springs, chemical environment varies from acid & oxidizing to alkaline & reducing.	Schmidt, 1950	Schmidt notes that "acid sulfate" phase of alteration at Goldfield is equivalent to the kaolinite-alunite-quartz alteration seen in active hot-springs, both the result of largely unmodified magmatic gases. Further notes clay alteration by steam-heated groundwaters.
1947-1963 Sulfur content of sulfide assemblages: implications for chemical potential of S	Sulfide assemblages with a high sulfur-content denote a high chemical potential of sulfur.	Sales and Meyer, 1949; McKinstry, 1959, 1963	The sulfur content of an assemblage is not an intensive variable. Therefore, this implication is correct only if metal ratio in successive assemblages (in this case Cu:Fe at Butte, Montana) does not change, a situation unlikely to be the general case, as noted by Gustafson (1963).
	Increasing sulfur content of assemblages in paragenetic sequence implies increasing chemical potential of S through time.	Sales and Meyer, 1949; McKinstry, 1959, 1963	
1967 "Sulfidation"	Formation of an assemblage of higher sulfur-content.	Meyer and Hemley, 1967	As defined, term does not require an increase in $f S_2$. For example, the reaction magnetite + 3 S_2 = 3 pyrite + 2 O_2 can proceed isothermally on decreasing $f S_2$ if $f O_2$ decreases sufficiently.
Path of "increasing sulfidation"	Assemblages at Butte record an increase in both $f S_2$ and $f O_2$ with time from early py-bn-cp to late py-cv-dg.[1]	Meyer and Hemley, 1967	First integration of mineral assemblages and geochemistry to arrive at evolutionary path for hydrothermal fluids in porphyry and vein systems in context of sulfidation and oxidation states.

1967 Link between $f\,S_2$ and $f\,O_2$	Relatively high acidity, high $f\,S_2$ and $f\,O_2$ at high ratios of $f\,S_2/f\,O_2$ are implied by assemblages such as py-cv-dg.	Meyer and Hemley, 1967	Solution composition commonly remains close to $H_2S = H_2SO_4$ boundary. If, on cooling, H^+ generation accelerates, the cooling path will diverge toward higher $f\,S_2$ and then trend back toward the rock buffer (i.e., the "looping path").[2]
1960-1970 "Sulfidation reaction"[3]	A reaction that produces a new assemblage of higher sulfidation state (not necessarily one of higher sulfur-content)	Barton et al., 1960; Barton and Skinner, 1967; Barton, 1970	Term generally applied to reactions that involve sulfur in the form of hypothetical S_2 gas and that appear as univariant lines on a log $f\,S_2$ - 1/T diagram. Example: 2 $FeS + S_2 = 2\ FeS_2$. Conceptually analogous to oxidation/reduction reactions involving O_2 or H_2; distinct from "sulfidation" (formation of an assemblage of higher sulfur content).
"Sulfidation state"[4] (of sulfide assemblages and fluids)	**A function of both $f\,S_2$ and T, the sulfidation state is defined relative to experimentally determined sulfidation reactions.**	Barton et al., 1960; Barton and Skinner, 1967; Barton, 1970	**Sulfide "petrogenetic grid" (log $f\,S_2$ – 1/T) introduced, describing a continuum of sulfidation states, which can increase or decrease during fluid evolution. General path on cooling is deduced to be one of increasing sulfidation state (Barton's 1970 "Main Line").**
1977-1987	Mineral assemblages at Creede, Colorado, indicate predominance of SO_2.	Barton et al., 1977	Determined activities of S_2 and O_2, pH, total S, in equilibrium with hm, py, Fe-chl, relatively oxidized assemblage.
SO_2/H_2S gas ratios "sulfur-gas buffer"	Ratios of dominant magmatic sulfur gases are near unity, an equilibrium that, if maintained, is an oxidizing $f\,O_2$ – T cooling path relative to FMQ or HM buffers.	Burnham and Ohmoto, 1980; Giggenbach, 1987	SO_2/H_2S fugacity ratio of magmatic vapor phase andesitic magmas ranges from 0.1 to 10; in absence of wall-rock exchange, ratio may remain unchanged as vapors cool to 500 to 350ºC.
	Magmatic gas ratios calculated from data on Fe-Ti-oxide and pyrrhotite compositions.	Whitney and Stormer, 1983; Whitney, 1984	SO_2/H_2S fugacity ratios for the Fish Canyon tuff, San Juan Mtns, Colorado, range from 0.6 to 2.9, average 1.6.

1981-1994	Classification of porphyry-related systems based on sulfidation & oxidation state of mineral assemblages combined with ore morphology.	Einaudi et al., 1981; Einaudi, 1982	Oxidized (porphyry-Cu, Cu-skarns,) vs reduced (Sn-W porphyries, W skarns) based on mineral assemblages; correlation with magma types. Sulfidation state contrasts between endmember porphyry-Cu (intermediate sulfidation state) and porphyry-related base-metal vein/replacement deposits (high and very high sulfidation states).
Classification of porphyry-related and epithermal deposits	Epithermal deposits classed by mineralogy and deduced fluid chemistry into "Adularia-Sericite" and "Acid Sulfate".	Bethke, 1984; Hayba et al., 1985; Heald et al., 1987	Endmember chemical environments proposed for epithermal deposits with implications for sulfidation & oxidation states: adularia-sericite relatively lower sulfidation-oxidation state than acid-sulfate deposits.
	Epithermal deposits classed by high (HS) vs low (LS) oxidation (valence) states of sulfur (n) in the fluid (e.g., n = +4 in SO_2 and n = -2 in H_2S).	Hedenquist, 1987; White and Hedenquist, 1990	Proposed that an intrinsic characteristic of the fluid of the two end-members be used for classification: acidic and oxidized vs neutral pH and reduced. Terminology does not relate directly to sulfide mineralogy or sulfidation state, yet it results in classification of epithermal deposits similar to acid-sulfate (HS) and adularia-sericite (LS).
	Epithermal deposits classed by dominant sulfides and deduced fluid chemistry into "high sulfidation" (HS) and "low sulfidation" (LS) types.	Hedenquist et al., 1994a	Noted that typical sulfide assemblages in these two end-member systems consisted of pyrite-enargite and pyrite±pyrrhotite with a variety of base metal sulfides, i.e., relatively high and low sulfidation states, respectively, as defined by Barton and Skinner (1967).
High (HS), intermediate (IS), and low sulfidation (LS) epithermal deposits	Classification of epithermal deposits based on tectonic settings, igneous associations, sulfidation state, and oxidation state.	John et al., 1999; Hedenquist et al., 2000; John, 2001	Integration of tectonic settings, intrinsic oxidation state of magmas, and mineralogy of deposits leads to a proposed continuum of sulfidation states in HS and IS epithermal deposits, contrasted with distinct LS deposits.

[1] for mineral abbreviations, see Table 4.
[2] See Meyer and Hemley (1967), p. 231-232 and their Fig. 6.9.
[3] See Barton and Skinner (1967, 1976) for an authoritative review of the geochemistry of sulfide minerals.
[4] Definition of sulfidation state used in present paper, with respect to mineral assemblages and fluids.
This table is restricted to the porphyry and epithermal environments and to processes & concepts related to volatile components and their link to sulfidation state; it thereby leaves out important contributions on topics of ore-depositional processes, evidence from light stable isotopic and fluid inclusion studies, and classifications based on morphology or metal content.

Table 2. Sources of data on the oxidation and sulfidation states of magmas plotted on Figures 3, 4, and 5

Name in Figure keys	Location	Geologic Province/Tectonic Setting	Magma Series	Rock Type	Source for oxidation State (Rh)	QUILF used to recalculate T and fO2[1]	Source for sulfidation state (Rs)[2]
Volcanic Rocks							
Pinatubo	Western Luzon, Philippines	Active Island arc	CA	D	Imai et al. (1993)	No; authors use QUILF	no data
Rabaul	New Britain, Papua New Guinea	Active Island arc	CA	A, D, R	Heming and Carmichael (1973)	No; authors use QUILF	Heming and Carmichael (1973)
Satsuma-Iwojima	Kikai caldera, Japan	Active Island arc	CA	D	no data		Ueda and Itaya (1981)
Nevado del Ruiz	Central Cordillera, Colombia	Active Continental arc	CA	A, D	Fournelle (1990); Melson et al. (1990)	Yes	no data
St. Helens	Mount St. Helens, Cascades, Washington, USA	Active Continental arc	CA	D	Melson and Hopson (1981)	Yes	Nordlie et al. (1983)
Bishop Tuff	Long Valley caldera, California, USA	Continental, transtensional	CA	R	Hildreth (1977)	Yes	Hildreth (1977)
Fish Canyon	La Garita caldera, Colorado, USA	Central San Juan volcanic Field	CA	QL	Xirouchakis et al. (2001)	Authors provide lower limit based on QUILF	Whitney and Stormer (1983)
Julcani	Peru	Continental arc	KCA	D, R	Drexler and Munoz (1988)	Yes	Drexler and Munoz (1988)
Western Andesite	Great Basin, Nevada (Tonopah, Paradise Range and Kate Peak) and Walker Lane, California (Bodie Hills), USA	Continental arc, transtensional	KCA	A, D, R	John (2001)	Author uses QUILF	no data
Northern Nevada Rift	Great Basin, Nevada & Oregon, USA	Continental rift	KT	B, BA, R	John (2001)	Author uses Quilf	no data
Taupo & Coromandel	North Island, New Zealand	Taupo Volcanic Zone, Coromandel peninsula	CA	RD	Rutherford and Heming (1978)	Yes	Rutherford and Heming (1978)
Azores – Canary Islands	Mid-Atlantic Ridge, Spain	MOR related fracture zones	A	B	Wolff and Storey (1983)	Yes	Wolff and Storey (1983)
Plutonic Rocks							
La Gloria	Central Chilean Andes, Chile	Continental magmatic arc	KCA	GD, QM	Cornejo and Mahood, (1997)	Yes	no data
Yerington	Yerington batholith, Nevada, USA	Continental magmatic arc	CA	GD, QM	Dilles (1987)	Yes	no data
Wasatch-Oquirrh	Wasatch (Park	Continental back-	KCA	M	Core (2001)	Yes	no data

| | Premier stock) and Oquirrh (Last Chance stock) Mountains, Utah | arc | | | | | |
| Oslo Rift | Central & Southern Oslo Rift, Norway | Continental rift | A | M | Neumann (1976) | Yes | no data |

[1] QUILF (Andersen et al., 1991; Andersen et al., 1993) was used to recalculate temperature and log fO_2 from data on assemblages involving pyroxenes, iron-titanium oxides and titanite given in the references listed. Log fO_2 values were then converted to Rh (Rh ≈ log [X H_2 / X H_2O]) using equation 15.6 of Giggenbach (1997).

[2] LogfS_2 – 1/T values for volcanic rocks are taken from the references listed, without recalculation, and converted to Rs (Rs ≈ log [X H_2 / X H_2S]) using the relations 2 $H_2S_{(g)}$ = 2 $H_{2,(g)}$ + $S_{2,(g)}$ from SUPCRT92 (Johnson et al., 1992).

Magma series abbreviations: A = alkalic, CA = calcalkalic, KCA = high-K calcalkalic, KT = high-K tholeiitic

Rock type abbreviations: see Table 3.

Table 3. Measured compositions of vapors discharged from volcanic fumaroles, magmatic-hydrothermal and geothermal fumaroles, plus total discharge from some geothermal wells.

System	Location	Rock type [1]	T (°C)	H_2O [2]	CO_2 [2]	SO_2 [2]	H_2S [2]	HCl [2]	HF [2]	H_2 [2]	R_H [3]	R_S [4]	R_{SH} [5]	Refs [7]
Volcanic fumaroles														
Erta'Ale	Ethiopia	AB	1130	794000	104000	67800	6200	4200	na	14900	-1.73	0.38	1.04	a,b
Galeras	Colombia	D	642	914800	59800	8415	5725	7160	620	2850	-2.51	-0.30	0.17	a,g
Klyuchevskoy	Kamchatka	B	1100	977300	1200	900	20	14200	2500	5900	-2.22	2.47	1.65	a,k
Momotombo	Nicaragua	BA	844	950500	23800	7000	4900	3500	290	8700	-2.04	0.25	0.15	a,h
Mt. Usu	SE Hokkaido	D	690	993000	3600	320	180	340	60	2000	-2.70	1.05	0.25	a,f
Ngauruhoe	New Zealand	A	640	960000	16050	10200	6800	2500	na	1420	-2.83	-0.68	0.18	a
Papandayan	Indonesia	A	400	959000	29360	6750	2900	1250	33	140	-3.84	-1.32	0.37	a,e
St. Helens [6]	Washington	D	650	986000	8800	670	900	700	200	4000	-2.39	0.65	-0.13	o
Satsuma Iwojima	S Kyushu	R	877	973600	5095	8180	1640	5306	277	6070	-2.21	0.57	0.70	a,I
Showa Shinzan??	SE Hokkaido	D	800	980000	12000	430	4	530	240	6300	-2.19	3.20	2.03	a,j
Vulcano	Italy	TB	620	861000	119000	6800	4800	4530	1010	1510	-2.76	-0.50	0.15	a
White Island, 84	New Zealand	D	760	927000	52900	8150	2450	5180	300	3020	-2.49	0.09	0.52	c,d
White Island, 84	New Zealand	D	457	941000	29100	13200	3300	12450	na	540	-3.24	-0.79	0.60	d
White Island, 88	New Zealand	D	495	920000	60100	10000	6000	2400	28	400	-3.36	-1.18	0.22	a,f
Augustine [6]	Alaska	D	870	847700	22700	61800	6800	10100	860	5400	-2.20	-0.10	0.96	x
Etna [6]	Italy	AB	928	919000	14000	28000	na	25000	5000	7000	-2.12	na	na	o
Kudryavy, 91	S Kurils	BA	870	921000	27000	23300	5800	6600	610	13000	-1.85	0.35	0.60	m
Kudryavy, 91	S Kurils	BA	585	951000	24900	11800	3900	5000	570	1700	-2.75	-0.36	0.48	m
Lewotolo	Lomblen, NTT	A	490	766000	120000	77700	9200	1260	369	540	-3.15	-1.23	0.93	y
Merapi	Java	A	900	940000	43000	5000	5000	2000	100	5000	-2.27	0.00	0.00	w
Tolbalchik	Kamchatka	B	1020	979400	200	1100	300	10400	3000	5500	-2.25	1.26	0.56	v
Unzen	N Kyushu	A	818	955000	27000	4370	2430	2610	na	7740	-2.09	0.50	0.25	u
Magmatic hydroth.														
El Chichon, 83	Mexico	TA	115	992400	7100	170	240	250	na	140	-3.85	-0.23	-0.15	n
El Chichon, 95	Mexico	TA	101	841600	142600	400	2200	400	6	1040	-2.91	-0.33	-0.74	n
El Ruiz	Colombia	A	82	955000	23400	19800	1760	59	<10	86	-4.05	-1.31	1.05	a,e
Kuju Iwoyama, 61	S Kyushu	R	400	969000	4500	6900	14100	4800	970	1000	-2.99	-1.15	-0.31	p
Kuju Iwoyama, 84	S Kyushu	R	320	993000	910	1800	2800	1200	42	28	-4.55	-2.00	-0.19	p
Kuju Iwoyama, 84	S Kyushu	R	165	992000	1800	2200	2600	1800	67	5	-5.30	-2.72	-0.07	p
Kudryavy, 91	S Kurils	BA	130	950000	22500	23000	2600	110	5	20	-4.68	-2.11	0.95	m
Manza karabuki	NE Honshu	A	94	992000	1460	220	6290	20	na	0.54	-6.26	-4.07	-1.46	z
Mutnovsky funnel, 83	Kamchatka	BA	360	987000	5190	4020	1640	975	260	884	-3.05	-0.27	0.39	a,l
Mutnovsky S bottom, 83	Kamchatka	BA	106	981000	13585	1045	2740	60	1	106	-3.97	-1.41	-0.42	l
Mutnovsky upper, 83	Kamchatka	BA	272	988000	9820	290	1020	160	10	350	-3.45	-0.46	-0.55	l
Mutnovsky N bottom, 83	Kamchatka	BA	97	978000	12400	2400	6310	550	9	110	-3.95	-1.76	-0.42	l
Nasu mugen	NE Honshu	A	149	996000	2980	120	520	60	na	26	-4.58	-1.30	-0.64	z
Showa Shinsan	SE Hokkaido	D	336	998900	420	34	45	260	na	340	-3.47	0.88	-0.12	c
Vulcano crater	Italy	TB	285	918000	69000	2950	2850	6700	na	10	-4.96	-2.45	0.01	j
Vulcano beach	Italy	TB	100	910760	86430	nd	1920	nd	nd	94	-3.99	-1.31	na	q
White Island, 84	New Zealand	D	197	947000	40600	3760	840	7260	na	21	-4.65	-1.60	0.65	c,d
White Island, 84	New Zealand	D	106	951000	44200	1820	2080	60	na	19	-4.70	-2.04	-0.06	c,d
White Island, 84	New Zealand	D	100	960000	36300	270	1730	260	na	122	-3.90	-1.15	-0.81	d
Zao	NE Honshu	A, D	96	977000	19800	2400	120	nd	na	4.3	-5.36	-1.45	1.30	z
Geothermal														
Campi Flegrei	Italy		155	845000	153000	na	1780	31	na	226	-3.57	-0.90	na	c
Darajat	Java	A	104	942000	54000	nd	2440	87	na	945	-3.00	-0.41	na	c
Krafla	Iceland	B	300	985000	13150	nd	350	nd	na	360	-3.44	0.01	na	c
Ketetahi	New Zealand	A	136	956400	37800	nd	1300	nd	na	1020	-2.97	-0.11	na	c

System	Location	Rock type[1]	T (°C)	H_2O[2]	CO_2[2]	SO_2[2]	H_2S[2]	HCl[2]	HF[2]	H_2[2]	R_H[3]	R_S[4]	R_{SH}[5]	Refs[7]
Broadlands well 25	New Zealand	R/D	290	994900	4890	nd	47	nd	nd	9	-2.88	0.23	na	r
Kawerau well 19	New Zealand	R, A	275	998300	1560	nd	65	nd	nd	5	-2.93	-0.10	na	s
Mokai well 6	New Zealand	R	319	998900	1015	nd	43	nd	nd	1.1	-4.21	-0.76	na	s
Rotokawa well 6	New Zealand	R	301	987600	2120	nd	120	nd	nd	9	-3.04	-0.22	na	s
Waiotapu well 7	New Zealand	R	242	999000	920	nd	53	nd	nd	5	-2.47	0.13	na	t
Wairakei well 72	New Zealand	R	260	999800	250	nd	10	nd	nd	0.7	-3.57	-0.08	na	r

[1] Abbreviations for igneous rocks: A = andesite, AB = alkali basalt, B = basalt, BA = basaltic andesite, D = dacite, GD = granodiorite, M = monzonite, QL = quartz latite, QM = quartz monzonite, R = rhyolite, TA = trachyandesite, TB = trachybasalt.

[2] µmols/mol

[3] R_H = log (XH_2 / XH_2O), where X = analytical mole fraction

[4] R_S = log (XH_2 / XH_2S), where X = analytical mole fraction

[5] R_{SH} = log (XSO_2 / XH_2S), where X = analytical mole fraction

[6] composition recalculated ("restored") by original author

[7] References: a, Giggenbach (1996); b, Giggenbach and LeGuern (1976); c, Giggenbach et al. (1986); d, Giggenbach (1987); e. Giggenbach et al. (1990); f, Giggenbach and Matsuo (1991); g, Martini (1993), h, Menyailov et al. (1986); i, Shinohara et al. (1993); j, Mizutani and Suguira (1982); k, Taran et al. (1991); l, Taran et al. (1992); m, Taran et al. (1995); n, Taran et al. (1998); o, LeGuern (1988); p, Mizutani et al. (1986); q , Chiodini et al. (1995); r, Giggenbach (1980); s, Giggenbach (1995); t, Hedenquist and Browne (1989); u, Ohba et al. (1994); v, Menyailov et al. (1984); w, Allard (1983); x, Symonds et al. (1990); y, Poorter et al. (1991), z, Kiyosu (1983)

Note: vapors from magmatic hydrothermal systems interact with acidic fluid; geothermal vapors derive from near-neutral pH fluid. R_H and R_S values for geothermal wells calculated using vapor-liquid distribution coefficients (Giggenbach, 1980) to allow comparison of total well discharge compositions to vapors discharged from fumaroles.

na, not available; nd, not detected

Table 4: Summary of alteration and sulfide mineral assemblages in subalkaline porphyry-Cu[1], porphyry-related base-metal vein[2], and epithermal Au-Ag deposits.

Porphyry Cu Left to right: *time toward present and/or decreasing depth and/or distance increasing from center*[3]

examples	early age[3], higher T		intermediate age[3]	late veins[3], lower T,	references
Type 1 porphyry: major mt-dg-bn in highest grade Cu ore					
Batu Hijau; Panguna; Yerington mine	early mt (B, M)[4]; **mt+dg+bn, mt+bn+cp**[5] **(K)**	bn+cp, cp (K)	cp+py, mt (or hm)+cp (CS, QSP)	py+bn, sl+gl+tn (CC, CS)	Clode et al., 1999; Eastoe, 1978; Proffett, 1979
Type 2 porphyry: major mt-bn-cp in highest grade Cu ore					
Bajo de l'Alumbrera; Dos Pobres; Rosario Porphyry (under Rosario vein)	early mt (M, K); **mt+bn, mt+bn+cp (K)**	bn+cp (CC)	cp+py, hm(or mt)+cp (CS, QSP)	py+gl+sl (P); py+en (**AA**) Rosario vein	Ulrich & Heinrich, 2001; Langton & Williams, 1982; Dick et al., 1994
Type 3 porphyry: major to moderate dg-bn or bn-cp, mt absent or minor in highest grade Cu ore					
Bingham; Chuquicamata; El Salvador; Grasberg; Morrison	early mt (M, K), rare po+cp; **dg+bn+cp; bn+cp (EDM**[6]**, K)**	**cp+py, mt+cp+py**[5] **(B)**	cp+py, cp+py+bn (QSP); later cp+py+tn+ sl (IA)	(po+cp at Morrison); others: py+bn+en, py+en+cv (AA); latter is ore at Chuquicamata	John, 1978; Redmond et al., 2001; Ossandon et al., 2001; Gustafson & Hunt, 1975; Gibbins, 2000; Pollard & Taylor, 2002; Carson & Jambor, 1976
Type 4 porphyry: major cp-py, minor cp-bn or mt-cp-py in highest grade Cu ore					
Butte[7], Magma Porphyry (deep lateral to Magma Vein); Sierrita-Esperanza; Silver Bell; Sungun	early mt (M, B); bn+cp, cp, cp+py (EDM[7], K, B)	bn-cp, **cp, cp+py (K, B)**	**cp+py (QSP, CAS, SC)**	py (QSP); cp+py (C), cp+py+sl, gl (SC, CC); **ore at Butte & Magma: py+cc+dg+bn (AA); py+bn+cp (QSP)**	Manske and Paul, 2002; West and Aiken, 1982; Preece and Beane, 1982; Graybeal, 1982; Hezarkhani and Williams-Jones, 1998;

Porphyry-Cu Related Base-Metal Veins[2], *very high to intermediate sulfidation states*

examples	central or deep[3]	intermediate[3]		distal or shallow[3]	references
Butte Main Stage, (superimposed on porphyry-style ore)	py, cc, en, cv; py, cc, en	py, bn, cc, en; relicts of sl	py, cp, tn, (bn); relicts of sl	sl, (py, gl, rho); rho, (sl, py, gl); Ag, (gl, sl, rho, py)	Sales and Meyer, 1949; Meyer et al., 1968; Proffett, 1979
Chuqicamata Main Stage, (superimposed on early porph-style bn-cp, mt-cp)	Early: py, cp, bn; py, bn, dg, (en); Late: py, dg, cv, (en); en, (py, sl); en, sl, cv, dg; cv, dg, (py, hm)		py+cp+bn; py, bn, dg, (en); py, dg, cv, (en)	tn	Lopez, 1939; Ossandón et al., 2001
Rosario vein, Collahuasi (on top of Rosario porphyry)	py-cp-(tn), py-bn-(en), cc-dg-cv		cp, cp-py	py	Hunt, 1985; Dick et al., 1994; Clark et al., 1998

Epithermal Au-Ag: left to right: *time toward present and/or decreasing depth and/or distance increasing from center*

examples	alteration	sulfide temporal sequence		variation	references
High-Sulfidation epithermal: py-en veins, AA halos, Cu-rich, some affiliated with porphyry Cu deposits					
Lepanto (over porphyry), El Indio, Goldfield	VQ-AA QSP, py	en+lz+py	cp+tn+sl+g l ±py	late Au te or Ag sf	w/ time, or on margin	Hedenquist et al., 1998; Jannas et al., 1999; Ransome, 1909
La Mexicana, Lahóca, Summitville (all over	AA-VQ py	py+tn+cp ±Au	tn±en±fm, Au+py	py+en+ fm, Au te	w/ dec depth or	Losada-Calderón and McPhail, 1996; Gatter et al.,

porphyry)			or Au+ba	time		1999; Stoffregen, 1987

Intermediate-Sulfidation epithermal: base-metal sulfide & Ag-rich veins

Pachuca, Fresnillo, Creede, Comstock Lode	adul, QSP, IA, P	sl+gl+py+ cp+tt	Ag sf, ±cp, Au	sl FeS 1-25 mole%	w/ time or distance	Geyne et al., 1963; Gemmell et al., 1988; Barton et al., 1977

Low-Sulfidation epithermal: sulfide poor, Au (Ag) bonanza veins

Sleeper, Midas, McLaughlin, Hishikari	IA	py-mc	py+Au±na Ag sf, ch (sl, tt, cp)	late or shallow op, rl, cn	w/ time, multiple veins	Saunders, 1994; John et al., 1999; Sherlock et al., 1995; Izawa et al., 1990

[1] in porphyry-type deposits, the position of molybdenite is not included in this table, although in most deposits it post-dates the main stage of veinlet copper ores and predates the late base-metal veins

[2] additional examples and summaries of these deposits or ore-styles can be found in Einaudi (1982) and Bartos (1989)

[3] Asemblages listed are representative of the types of deposits. but not every deposit within a type contains all of the assemblages listed for that type. Only time-space diagrams can accurately portray evolution; in general, the early (high-T)-to-late(low-T) progression summarized here is from the perspective of the highly mineralized zone, but "late" or "distal" assemblages may be forming at the same time as "early" or "central" assemblages on the system scale. Also, early or high-temperature assemblages in porphyries commonly are repeated many times; high temperature = approx 550 to 400ºC; intermediate temperature = approx 350ºC; low temperature = approx 300 to 250ºC; epithermal deposits form around 250 to 200ºC.

[4] alteration types temporally associated with the sulfide assemblages in the porphyry and vein deposits are listed in parentheses; see abbreviations below.

[5] sulfide assemblages in bold represent the highest grade of copper in most of the porphyry deposits listed under a given type
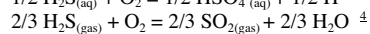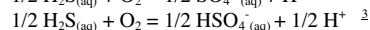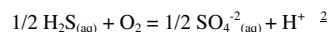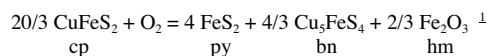
[6] in the deposits listed under Type 3, EDM is recognized only at Bingham

[7] refers to pre-Main Stage at Butte; in the deposits listed under Type 4, EDM is recognized only at Butte

Sulfide abbreviations: asp = arsenopyrite; bn = bornite; cc = chalcocite; cn = cinnabar; cp = chalcopyrite; dg = digenite; en = enargite; fm = famatinite; gl = galena; hm = hematite; lz = luzonite; mc = marcasite; mt, = magnetite; na = naumannite; op = orpiment; po = pyrrhotite; py = 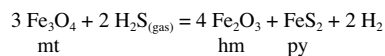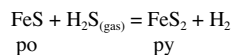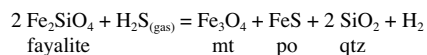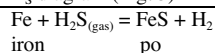pyrite; rl = realgar; sb = stibnite; sf = sulfosalts; sl = sphalerite; te = tellurides; tn = tennantite, tt = tetrahedrite

Gangue abbreviations: adul = adularia; ch = chalcedony; qz = quartz, rho = rhodocrosite; dol = dolomite

Alteration abbreviations: (AA) = "advanced argillic"; (AC) = albite-chlorite-calcite; (B) = biotite; (CAS) = chlorite-albite-calcite; (CC) = carbonate-chlorite-clay); (CS) = chlorite-sericite; (EDM) = "early dark micaceous", biotite, phengite, K-feldspar, andalusite, corundum; (IA) = "intermediate argillic", montmorillonite-kaolinite-illite, biotite chloritized, K-feldspar stable/metastable; (K) = "potassic", quartz, phlogopite, rutile, K-feldspar, anhydrite; (M) = amphibole-albite-magnetite; (P) = "propylitic", chlorite, epidote, calcite, albite; (QSP) = "phyllic, sericitic", quartz-sericite-pyite; (SCC) = sericite-chlorite-carbonate, (VQ) = vuggy quartz.

Table A. Reactions shown on R_H and R_S diagrams

R_H diagram (Fig. 3)

$3\ Fe_2SiO_4 + O_2 = 2\ Fe_3O_4 + 3\ SiO_2$
  fayalite   mt   qz

$2\ Ni + O_2 = 2\ NiO$

$2\ KFe_3AlSi_3O_{10}(OH)_2 + O_2 = 2\ KAlSi_3O_8 + 2\ Fe_3O_4 + 2\ H_2O$
      annite   K feldspar   mt

$3\ FeS + O_2 = 3/2\ FeS_2 + 1/2\ Fe_3O_4$
   po   py   mt

$3/2\ FeS + O_2 = 1/2\ Fe_3O_4 + 3/2\ S$
    po   mt   sulfur

$4/3\ FeS_2 + O_2 = 2/3\ Fe_2O_3 + 8/3\ S$ [1]
    py   hm   sulfur

$4\ Fe_3O_4 + O_2 = 6\ Fe_2O_3$ [1]
   mt   hm

$20/3\ CuFeS_2 + O_2 = 4\ FeS_2 + 4/3\ Cu_5FeS_4 + 2/3\ Fe_2O_3$ [1]
     cp   py   bn   hm

$1/2\ H_2S_{(aq)} + O_2 = 1/2\ SO_4^{-2}{}_{(aq)} + H^+$ [2]
$1/2\ H_2S_{(aq)} + O_2 = 1/2\ HSO_4^-{}_{(aq)} + 1/2\ H^+$ [3]
$2/3\ H_2S_{(gas)} + O_2 = 2/3\ SO_{2(gas)} + 2/3\ H_2O$ [4]

R_S diagram (Fig. 5)

$Fe + H_2S_{(gas)} = FeS + H_2$
iron   po

$2\ Fe_2SiO_4 + H_2S_{(gas)} = Fe_3O_4 + FeS + 2\ SiO_2 + H_2$
  fayalite   mt   po   qtz

$FeS + H_2S_{(gas)} = FeS_2 + H_2$
 po   py

$3\ Fe_3O_4 + 2\ H_2S_{(gas)} = 4\ Fe_2O_3 + FeS_2 + 2\ H_2$
   mt   hm   py

$5\ CuFeS_2 + 2\ H_2S_{(gas)} = Cu_5FeS_4 + 4\ FeS_2 + 2\ H_2$
  cp   bn   py

$H_2S_{(gas)} = S + H2$ [5]
    Sulfur

Calculated at 500 bars pressure, unless noted
[1] these reactions are adjusted in Figs. 2 - 8 to be compatible with magnetite + hematite equilibrium data from Myers and Eugster (1993)
[2] defines the predominance boundary for aqueous sulfur species at pH = 6 (this pH is approximately neutral in the epithermal temperature range)
[3] defines the predominance boundary for aqueous sulfur species at pH = 3
[4] used to define the "sulfur-gas buffer" at 1, 30, and 1000 bars based on data in Giggenbach (1987)
[5] defines saturation with respect to liquid sulfur, "sulfur condensation"

Mineral abbreviations as in Table 4.